GA–A23877

DIRECT ENERGY CONVERSION FISSION REACTOR

ANNUAL REPORT FOR THE PERIOD AUGUST 15, 2000 THROUGH SEPTEMBER 30, 2001

by
L.C. BROWN

Work supported by
Nuclear Energy Research Initiative (NERI)
Program No. DE-FG03-99SF21893 for
the U.S. Department of Energy under

JANUARY 2002

DISCLAIMER

GA–A23877

DIRECT ENERGY CONVERSION FISSION REACTOR

ANNUAL REPORT FOR THE PERIOD AUGUST 15, 2000 THROUGH SEPTEMBER 30, 2001

by
L.C. BROWN

Work supported by
Nuclear Energy Research Initiative (NERI)
Program No. DE-FG03-99SF21893 for
the U.S. Department of Energy under

GENERAL ATOMICS PROJECT 30033
JANUARY 2002

TABLE OF CONTENTS

LIST OF FIGURES

LIST OF TABLES

EXECUTIVE SUMMARY

Sandia National Laboratories, Los Alamos National Laboratories, The University of Florida, Texas A&M University and General Atomics have undertaken a joint project to explore the possibilities of exploiting direct energy conversion to increase the efficiency of electricity production from fission nuclear reactors. This report describes only the work performed at General Atomics during Phase 2 of this three-year project. Sandia National Laboratories leads the overall project and provides overall project reporting.

During Phase 1, the number of direct energy conversion concepts under investigation was reduced to three: Magnetic Collimator Fission Reactor, Quasi-Spherical Magnetically Isolated Fission Electric Cell Reactor and Fission Enhanced MHD Vapor Core Reactor. During Phase 2, each of the concepts has been further refined. Each of the concepts was championed by a particular laboratory:

1. Magnetic Collimator Fission Reactor — Texas A&M University,
2. Quasi-Spherical Magnetically Isolated Fission Electric Cell Reactor — Sandia National Laboratories
3. Fission Enhanced MHD Gaseous Core Reactor — University of Florida. Los Alamos and General Atomics provided support to all three concepts in areas where they have specific expertise.

General Atomics supported the Phase 2 effort in three major areas:

1. Thermal performance model of the refrigeration systems required for the superconducting magnets of the fission electric cell and magnetic collimator,
2. Stability of the fission cell cathode assembly relative to asymmetric electric forces
2. Design of the fuel recycle loop, including fission product removal, for the vapor core reactor.

1. INTRODUCTION

Direct energy conversion (DEC) for fission may be defined, in a broad sense, as the production of electrical energy from a fission nuclear reactor without the use of a mechanical energy conversion device. In its purest form, DEC directly converts the kinetic energy of fission fragments into electrical energy and is the only potential means for producing electrical energy from a fission reactor without the Carnot efficiency limitations. This project was undertaken by Sandia National Laboratories, Los Alamos National Laboratories, The University of Florida, Texas A&M University and General Atomics to explore the possibilities of exploiting direct energy conversion. In the initial scoping studies a number of DEC techniques were explored, as well as techniques that use direct fission energy to augment a more traditional energy recovery scheme. Phase 1 ended with the selection of two pure DEC techniques and one hybrid scheme. The pure DEC techniques, Quasi-Spherical Magnetically Isolated Fission Electric Cell Reactor (QSMIFECR, or ECR for short) and Magnetic Collimator Reactor (MCR), were proposed by Sandia. The University of Florida proposed the Vapor Core Nuclear Reactor (VCR), which makes peripheral use of the direct fission product energy. Sandia National Laboratories leads the overall project and provides overall project reporting and documentation.

Both the ECR and the MCR directly convert the kinetic energy of the fission products into electrical energy by slowing the positively charged fission products with an electric field. The electric field, on the order of 2 MV, is self-generated by the transport of the fission products from the fuel cathode to the anode. The electric energy is extracted from the flow of electrons from the cathode to the anode through an external electric circuit. Since any kinetic energy lost through collisions of fission products within the fuel results in heat deposited in the cathode instead of electrical energy extracted from the particles, the fuel must be thin so that all the fission products can escape with minimal collisions. The fuel thickness must be on the order of a micron or less for significant direct energy conversion to take place. Moreover, if the fuel is supported by any thickness of inert material, the efficiency will be decreased by the thermal energy of the fission product deposited in the support.

The ECR is composed of many individual cells (Fig. 1), each composed of a fuel cathode and a moderator anode. Ideally, the cathode would be a point of fuel at the center of the anode, so that all fission products would travel along radii of the anode, always normal to the electric field. Since the volume of the fuel would be zero for this idealized geometry, the concept under investigation has the fuel in the form of a thin spherical shell

and the cathode radius is a significant fraction of the anode radius. As the cathode radius approaches the anode radius, the reactor can contain more fuel but a larger fraction of the fission product kinetic energy is not directed normal to the electric field and thus becomes heat. Since the cathode must be connected to the anode through an external electric circuit there must be a penetration through the anode for the cathode lead wire. To minimize the number of connections, many cathodes are spaced along each support wire, which also serves at the electrical lead. The anode, which surrounds each cathode, has two axial penetrations, somewhat larger than the diameter of the cathode, so that a cathode assembly can be inserted into each anode. To prevent direct flow of electrons across the gap between the electrodes, the cathodes are insulated from the anodes by two separate mechanisms: each individual cell is insulated by an axial magnetic field provided by a superconducting magnetic solenoid wound around the entire reactor; and a sufficient length of insulator is placed at both ends of each cathode assembly to prevent electrical breakdown on the surface of the insulator.

The MCR is similar to the ECR in that the entire reactor is within a superconducting solenoid. The fuel for the MCR is in the form of fine wires or thin tubes that are aligned along the magnetic field lines. Fission fragments exiting the fuel are constrained to a spiral path along the magnetic field line. After exiting the reactor, the fission fragments are retarded by an electric field and collected at the cathode. Any electron accompanying the fission fragments is repelled by a grid located between the reactor and the anode.

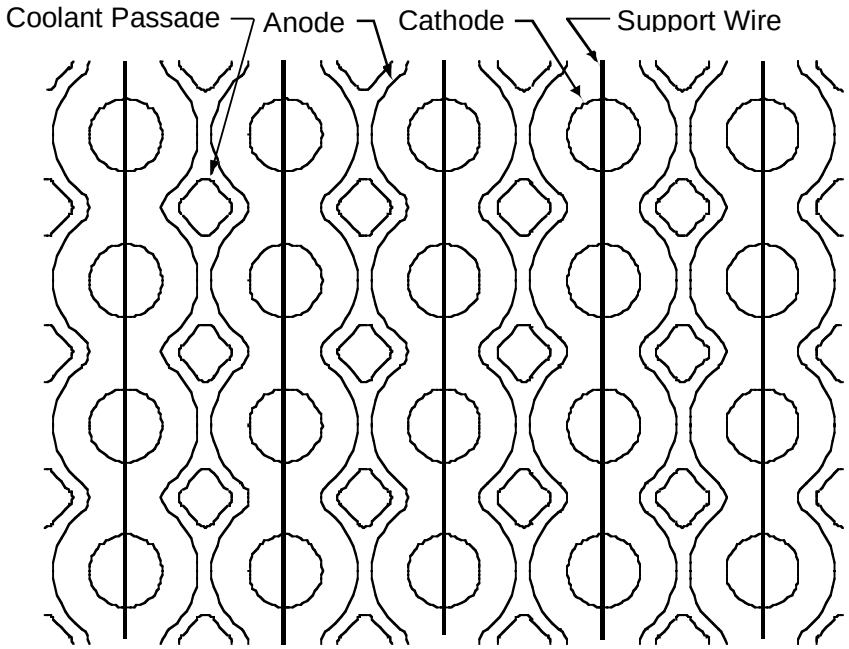

Fig. 1. Cross section of Quasi-Spherical Magnetically Insulated Fission Electric Cell Reactor.

The Vapor Core Reactor is only marginally a direct energy conversion concept as the majority of the fission energy is converted to heat and recovered by means subject to the Carnot limitations but the reactor temperature is very high so the theoretical efficiency is quite high. The reactor consists of a core of uranium tetrafluoride vapor and helium gas operating at 2500 K with a beryllium reflector. The gaseous core temperature is high but the structural and containment materials are cooled to more reasonable temperatures. The temperature of the gas exiting the reactor is too high for conventional turbines so the high temperature energy is extracted using magnetohydrodynamics (MHD). The uranium is still undergoing delayed fission as it passes through the MHD generator, providing the needed ionization. This ionization energy is the direct energy conversion component of the concept. A helium turbine-generator and a steam turbine-generator are used to extract additional energy at lower temperatures from the gas exiting the MHD generator.

This report documents the progress of General Atomics in support of the overall project. The work was done in three major areas:

1. Thermal performance model of the refrigeration systems required for the superconducting magnets of the Fission Electric Cell and Magnetic Collimator,
2. Stability of the Fission Electric Cell cathode assembly relative to electric forces, and
3. Design of the fuel recycle loop of the Vapor Core Reactor.

Each of these areas is independent of the others. What follows are essentially four independent reports on the four topics. Much of the detailed information is presented in appendices.

2. THERMAL PERFORMANCE OF A SUPERCONDUCTING COIL REFRIGERATION SYSTEM FOR DEC REACTORS

Both the Magnetic Collimator Reactor (MCR) concept and the Quasi-Spherical Magnetically Insulated Fission Electric Cell Reactor (ECR) concept require large magnetic fields to constrain electron motion. The magnitude of the magnetic fields is too great to be provided by permanent magnets and the losses from use of normal electromagnets would be large. Superconducting magnets only require power when initially establishing the field but some power is required for refrigeration to maintain the magnet at superconducting temperatures. A thermal performance model was developed for a superconducting magnet coupled to a refrigeration plant so that the energy requirements of the magnetic system could be estimated. The model was made available to Sandia in the form of an Excel spreadsheet. Sandia will use the model in the overall analysis of the MCR and ECR concepts.

Figure 2 indicates many of the important parameters of the model. The model considers a superconducting coil in a vacuum vessel insulated with multi-layer insulation (MLI). MLI consists of many layers of aluminum coated Mylar® film which is sewed into blankets. The films only touch infrequently so the primary mechanism for heat transfer in MLI is radiation. The MLI cannot bear significant load so the superconducting coil is supported within the insulation by G-10 fiberglass struts. Similar struts are required as earthquake restraints. The calculation begins with a specification of the solenoid length, the inside diameter of the vacuum vessel and a specification of the required magnetic field. The solenoid thickness can be determined from the magnetic field. Once the thickness of the insulation pack is specified, the rest of the geometry is defined. It might seem that the heat transfer to the coil could be reduced to any desired value by increasing the insulation thickness, but this is not the case. Increasing the insulation thickness causes the solenoid diameter to increase, both increasing the area for heat transfer and the weight of the solenoid. The cross sectional area of the struts is determined from the weight of the coil, thus thicker insulation ultimately results in higher heat transfer through the struts. The struts can be longer than the insulation thickness but their length cannot be more than the sum of the solenoid length and the insulation thickness. Varying the insulation thickness while maintaining the maximum strut length allows one to minimize the heat loss to the coil and thus optimize the solenoid package.

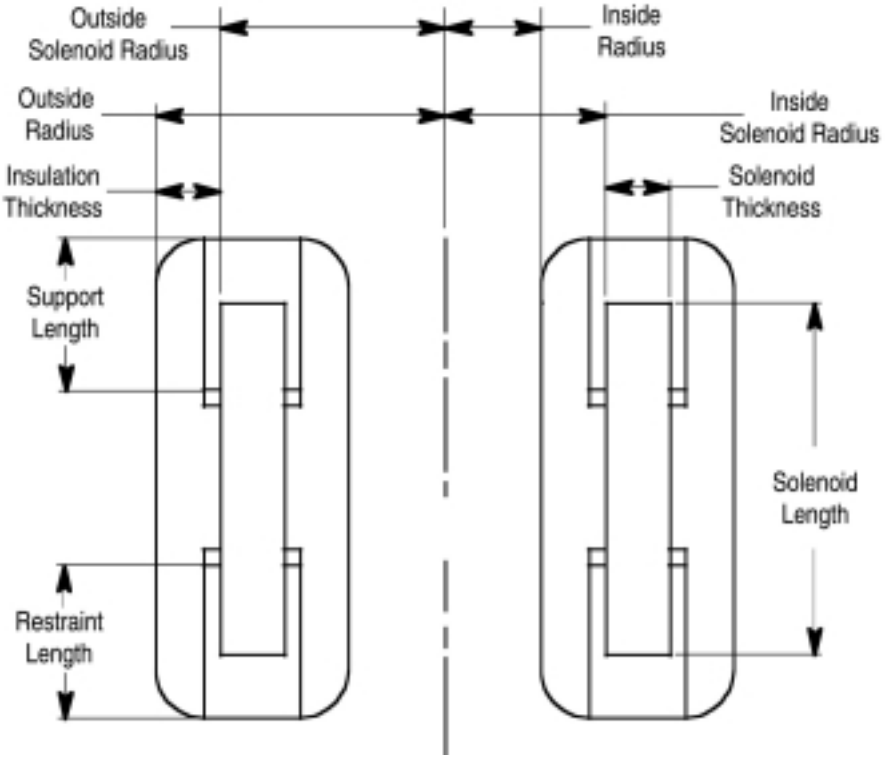

Fig. 2. Superconducting coil model geometry.

The heat transferred to the solenoid is removed by liquid helium. The power requirements can be reduced, at the penalty of a more complicated system, if both nitrogen and helium coolants are used. The optimization becomes a little more complicated as the location of the nitrogen-cooled intercept, within the insulation layer, must be determined. Data exist for the energy requirements of a refrigeration plant as a function of the refrigerant temperature and the required duty. This data was used to give the power requirements for a refrigeration plant with average and high efficiencies. Table 1 summarizes the input data and the results for a 3-meter diameter, 5-meter high Fission Electric Cell (FEC) coil and for the GA 30 MJ coil, one of the largest superconducting magnets ever fabricated. The 30 MJ coil was used to estimate the knockdown factor (the ratio of the heat loss through MLI in the fabricated coil to the heat loss calculated from MLI thermal conductivity). Using the average and high assumptions for refrigeration plant efficiency, the required power is in the range of 13.5 to 20 kW for the helium-cooled solenoid. If both liquid nitrogen and liquid helium cooling are employed, the cooling power can be reduced by 15%. Details of the model are given in Appendix A. In the final analysis, the refrigeration requirements are of little significance if a reactor of significant power can be built at the assumed size.

TABLE 1
COMPARISON OF SUPERCONDUCTING COIL PARAMETERS

	30 MJ Coil	FEC Coil
Central magnetic field (T)	3.92	2.5
Inside radius (vacuum vessel) — warm (m)	1.02	3
Solenoid length — Cold (m)	0.86	5
Coil temperature (K)	4.2	4.2
Pack current density (A/m^2)	15700000	30000000
G-10 support length (m)	0.25	1.5
Environment temperature (K)	300	300
Insulation thickness (m)	0.1	0.5
Knockdown factor for real world performance	*3*	*3*
Power required (average efficiency) (W)	13,717	22,028
Power required (high efficiency) (W)	8,447	13,528

3. STABILITY OF THE CATHODE ASSEMBLY IN A FISSION ELECTRIC CELL REACTOR

The Magnetically Insulated Quasi-Spherical Fission Electric Cell Reactor (ECR) consists of assemblies of very thin spherical cathodes, each one located inside a quasi-spherical anode. Each cathode assembly consists of a vertical support wire with cathodes located at a fixed pitch. See Fig. 1. The cathode assembly will be very long to minimize the amount of the reactor volume taken up with the anode-cathode insulation system at both ends of the assembly. If each cathode is exactly centered within its anode there is no side force on the cathode, but if there is any offset, e.g., due to manufacturing tolerances or a random vibration, the effect must be considered. Figure 3 shows the situation when all the cathodes, but one, shown in the middle, are centered in their anodes at V = 0. At 2 MV, the side force on the one off-center causes it to move even further off-center. Moreover, the other cathodes are also moved off-center from their initial positions by the resulting deflection of the support wire. ach of the displaced cathodes now contributes an additional side force to the cathode assembly and, thus, more deflection of the total system. The deflection can, in principle, be reduced to any desired amount by increasing the tension in the support wire.

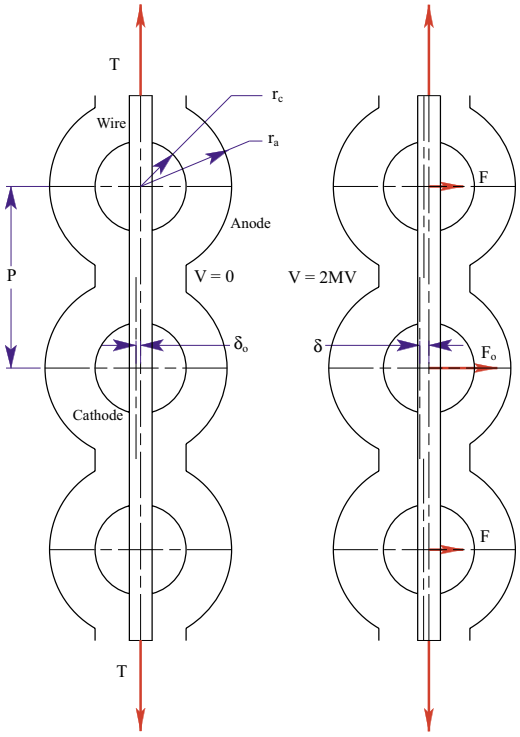

T = Tension in support wire
P = Pitch
r_c = Cathode radius
a_c = Anode radius
δ_o = Initial offset
δ = Final displacement
F_o = Initial side force
F = Induced side force

Fig. 3. Cathode assembly with an initial offset (δ_o) in the positioning of one anode/cathode pair.

Before beginning to analyze the cathode structure consisting of a series of cathodes on a support wire, it is instructive to calculate the tension required to restrain a single cathode in the center of a support wire with a length equal to the core height. The magnitude of the force and resulting tension may be approximated by

$$F(\delta) = \frac{\varepsilon_o \cdot \pi \cdot V_o^2}{2}\left[\left(\frac{r_c}{r_a - r_c - \delta}\right)^2 - \left(\frac{r_c}{r_a - r_c + \delta}\right)^2\right] \text{ and } T(\delta) = \frac{F(\delta)}{2 \cdot \sin\{\arctan[2\delta / P]\}} \quad ,$$

where ε_o is the permittivity of free space and V_o is the applied voltage.

As shown in Fig. 4, it takes an unreasonably large tension in the support wire to restrain the cathode if it is not exactly concentric with its anode. It is interesting to note that, while the side force is a continuous function, the required wire tension has a singular value of zero at zero offset, but it is large for any finite offset. The tension is so large that a support wire capable of restraining the single cathode is larger in diameter than the anode! Adding more cathodes and anodes in line can only make the situation worse.

Length of support wire	3 meters
Diameter of cathode	5.4 mm
Diameter of anode	9.6 mm
Minimum tension	131,150 Newton (29,490 lb_f)
Assumed tensile strength of wire	207 Mpa (30,000 psi)
Minimum wire diameter	28.4 mm

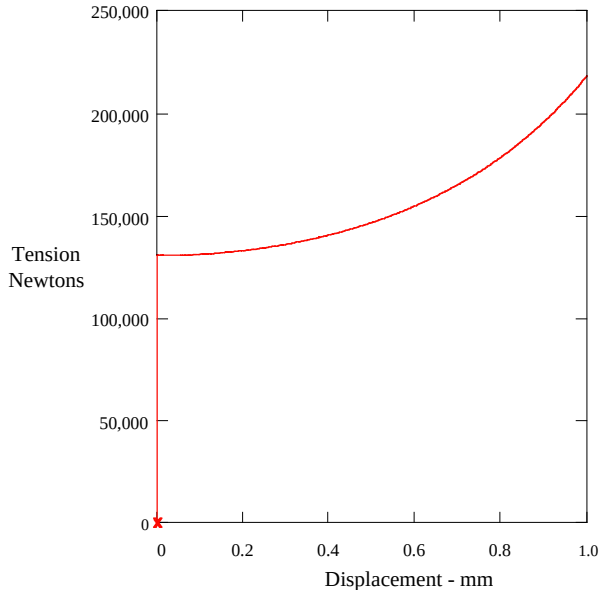

Fig. 4. Required tension in support wire to restrain a single cathode offset from center.

The source of the large tension is that the side force must be countered by the horizontal component of the tension in the support wire. The vector sum of the side force (F), the tension up the support (T_u) and the tension down the support (T_d) must be zero at rest. The tension vectors are almost normal to the side force, so the magnitude of the tension is many times that of the side force vector [Fig. 5(a)]. The obvious way to decrease the tension would be to introduce intermediate side supports so as to make the

angle between the side force vector and the tension vectors more obtuse [Fig. 5(b)]. Intermediate side supports would cause surface breakdown and would short any insulator. But a similar result can be obtained by introducing an intentional offset in the electric field at each anode-cathode pair such that each cathode is pulled away from the adjacent cathodes [Fig. 5(c)].

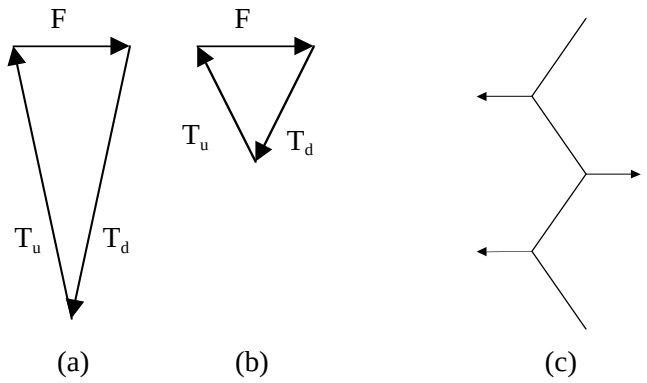

Fig, 5. Forces on the cathodes.

This is easy to visualize in two dimensions but it is also valid in three dimensions where the offset in the electric field is introduced progressively at 120 degree from cell to cell such that the support wire forms a spiral. The offset electric field may be obtained by offsetting the anodes in a spiral pattern, or, as shown in Fig. 6, by adding a feature, such as a "bump," to the inside of the anodes in a similar pattern.

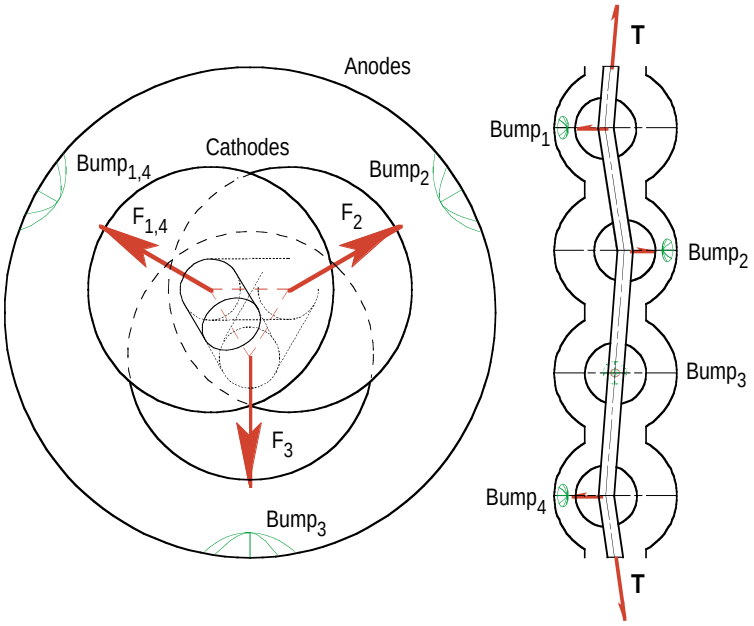

Fig. 6. Electrode configuration at 2 MV with spiral pattern of bumps on the anodes.

Wire tension at V = 2MV is plotted in Fig. 7 as a function of the final offset at equilibrium, for a selected initial offset of 0.1 mm at V = 0 V. In this example, the outer diameter of the cathodes is 5.4 mm, the inner diameter of the anodes is 9.6 mm, the vertical pitch between electrodes is 9.6 mm, and the stiffness of the wire is conservatively neglected. The left part of the plot shows that it would take an infinite tension to maintain the cathode in its initial offset position. The right part of the plot shows that it would take an infinite tension to prevent the cathode from contacting the anode. The plot also shows that, under the assumed conditions, the initial tension must be set larger than 589 N for the cathode to reach a stable equilibrium without being pulled into contact with the anode. A 1,004 N initial tension would provide a 70% force margin against such cathode instability**. S**electing a wire diameter of 1.5 mm would gives a tensile stress of 1,278 MPa (186 Ksi) in the wire, which may be within the capability of various high-strength steels and carbon fibers, depending on the temperature and irradiation conditions of the wire in operation. It should be noted that any tension larger than 589 N will result in force equilibrium at two different values of the final wire offset, e.g., at 0.173 mm and 1.18 mm final offset for a 1004 N tension.

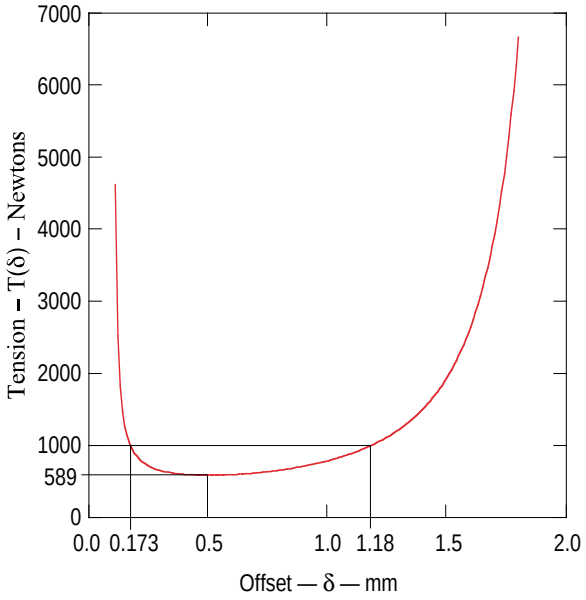

Fig. 7. Wire tension versus final offset for 0.1 mm initial offset.

A number of issues should still be investigated to determine the feasibility of the cathode/anode arrangement in a Fission Electric Cell reactor, among them the effects of:

- Wire bending stiffness. Taking it into account will slightly lower the required wire tension but it will add a bending stress to the tensile stress in the wire.

- Minimum gap between electrodes. From the electrical point of view, what is the minimum distance that must be maintained between the electrodes for the cell to operate properly?

- Dimensional tolerance effects on cathode positional stability. For example, if one of the has a different offset than the others, what is the effect on the force balance between the wire tension (T) and the side forces (F) on the cathodes? What would be required so that the string of cathodes can find a stable equilibrium without any cathode contacting its anode?

- Vibration effects on cathode positional stability. If the wire or the cathodes are subjected to time-varying forces or displacements, natural vibration modes of the cathode string may be excited. What would be required to prevent a cathode from moving so close to its anode that it could not be held back by the given constant tension in the wire, and would come into contact with its anode?

- Electrostatic forces effects on cathode structural integrity. Can the very thin cathode resist the stresses due to the electrostatic force distribution on the shell and the localized wire reaction? For example, with V = 2 MV, even if the electrodes were perfectly concentric, the electrostatic force distribution on the cathode would be equivalent to an 80 atm internal pressure. If it were resisted solely by the 0.4 μm-thick cathode shell, the tensile stress in the shell would be very high (~21,557 MPa or ~3,125 Ksi).

- Approximations in the force and stress calculations. The electrostatic force distributions on the electrodes and the resulting stresses in the cathodes and their support wire could be calculated more accurately by finite element analyses of the actual geometry and materials. If the results indicate that the arrangement is mechanically feasible, dimensions and materials could then be optimized.

4. SIMULATION OF THE GAS RECYCLE LOOP OF A VAPOR CORE REACTOR

4.1. Background

A process flow diagram (PFD) is the basic tool used to document a chemical process. The PFD consists of two parts: a flow diagram and stream table. The flow diagram shows and names each piece of process equipment and each process stream. The stream tables, which document the heat and material balance calculations, indicate the thermodynamic state of each stream including temperature, pressure, enthalpy flow rate and the material flow rates of each chemical species.

A model of the gas recycle loop of the Vapor Core Reactor (VCR) has been completed using the computer simulation program Aspen Plus, one of the premiere simulators used in the process industry. The simulator enables an engineer to create models of a process, and apply rigorous thermodynamic calculations using a variety of equations of state. The use of Aspen Plus facilitates the creation of a PFD that allows for study of permutations of a process relatively quickly. This PFD can be utilized in future work to produce more detailed PFDs and eventually piping and instrumentation diagrams (P&IDs). Applying process engineering to the VCR gas recycle loop specifically focuses the study on the energy flows associated with the separation of uranium tetrafluoride (UF_4) from the helium carrier gas, as well as separation and removal of fission products from the process.

The VCR simulation was based on a schematic diagram provided by Samim Anghaie to the DEC team, concentrating on the area within the box of Fig. 8. Process parameters were taken from the schematic where possible and are listed in Table 2. Additional parameters were required to begin the simulation and were estimated. These include the efficiencies of the MHD generator and He compressor, identification and concentration of fission products generated, and most importantly, the ratio of UF_4 to He exiting the gas core of the reactor.

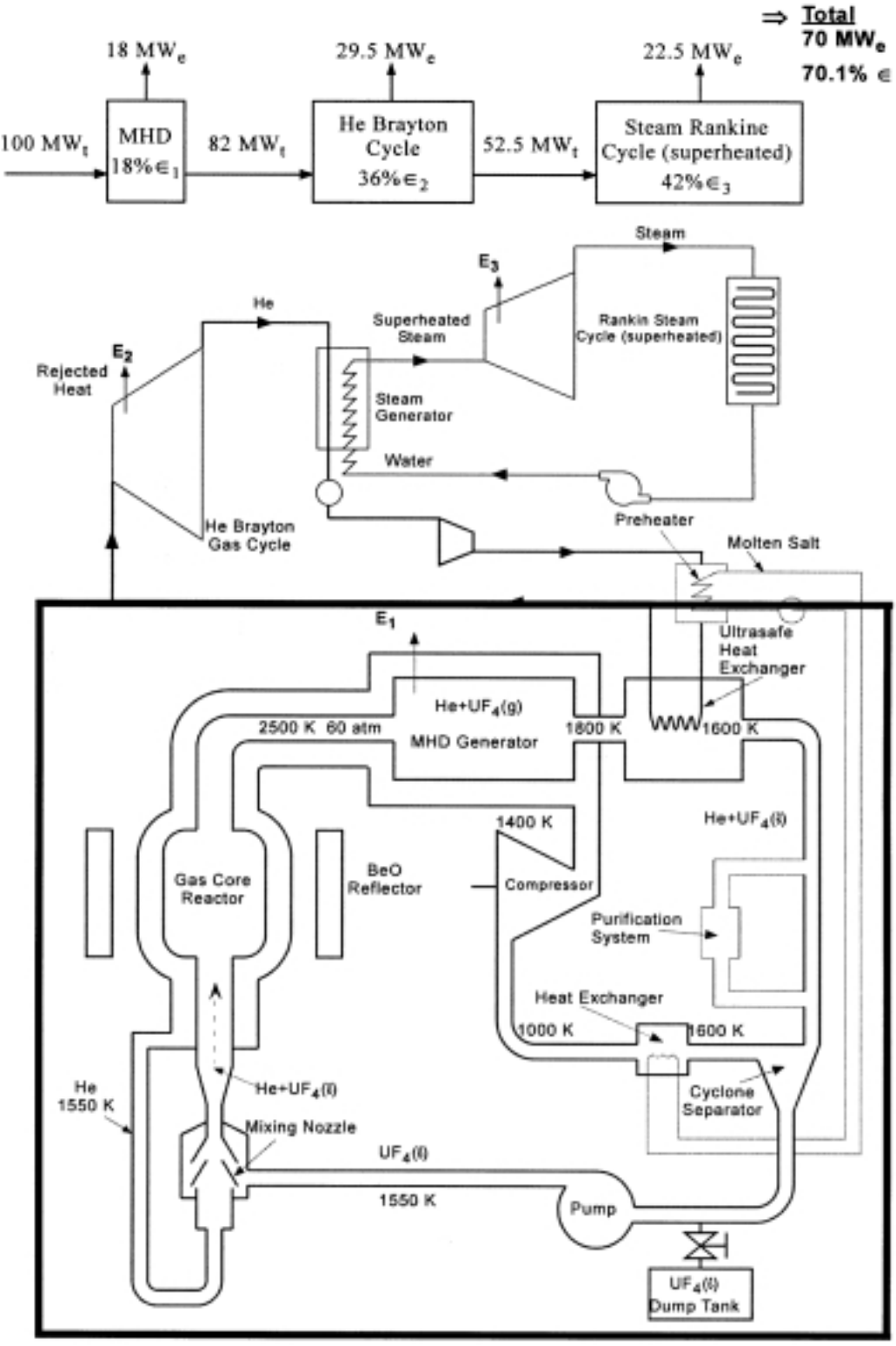

Vapour **C**ore **R**eactor With Combined **D**irect/Indirect **E**nergy **C**onversion (VCR-DEC)

Fig. 8. Schematic utilized for the VCR simulation.

TABLE 2
KEY PARAMETERS AND VALUES FOR SCHEMATIC DIAGRAM OF THE VCR

Gas core inlet/outlet temperature	1550 K, 2500 K	MHD generator outlet temperature	1800 K
Gas core outlet pressure	60 atm	MHD generator power output	18 MW
Gas core power output	100 MW	Ultrasafe heat ex. outlet temperature	1600 K
He compressor outlet temperature		1400 K	

The MHD generator was modeled as an isentropic turbine with an efficiency of 97%. An isentropic turbine is defined as having an expansion process that is reversible as well as adiabatic. This efficiency compares with the value of 93% used for He turbines in the Gas Turbine-High Temperature Gas-cooled Reactor (GT-HTGR). For the He Compressor, an isentropic compressor system with an efficiency of 88% and an initial pressure ratio of 1.73 was utilized, again close to the values used for the GT-HTGR. Fission products were estimated through calculation of fractional abundances, followed by research of available literature for compound properties. The fission products were then introduced into Aspen Plus as non-databank components. Detailed discussion of the fission products and resultant separation from the recycle loop can be found in Section 4.2 of this report. The missing information on the ratio of UF_4 to He exiting the gas core of the reactor was particularly daunting, as this ratio is the dominant factor in calculating separation parameters and power outputs throughout the simulation. Fortunately, differing ratios of UF_4 to He can be studied using the process simulator, and the ratios of 10 % to 60 % UF_4, stepped by 10%, were chosen for study.

4.2. Design

4.2.1. UF_4-He Separation

One of the first tasks in the simulation of the VCR gas recycle loop was to determine the appropriate properties for UF_4. While Aspen Plus did have the compound in its databank library, most of the information was focused on the solid phase. After researching available literature, the thermophysical properties presented by Samim Anghaie were chosen for modeling since this data focused on UF_4 fluid properties at relatively high temperatures (Anghaie, 1992). The significant properties utilized are available for review in Appendix B.

Preliminary process engineering focused on three main aspects: (1) separation of UF_4 from the He stream to below detectable limits, (2) interstage cooling and heat integration of the He compressor system, and (3) optimization of the temperature in the outlet stream from the Ultrasafe Heat Exchanger to maximize the temperature of the UF_4 entering the core of the reactor. A full PFD for the VCR gas recycle loop is available for review in Appendix B.

Initially, the outlet temperature from the Ultrasafe Heat Exchanger, designated PRIMHX, was set to the indicated value of 1600 K, but 28% of the UF_4 remained with the He stream after the first separator (SEP-1). Therefore it was necessary to provide three additional separators, (SEP 2-4), in order to remove UF_4 adequately from the He stream. The temperatures of the three separators were set to substantially eliminate the UF_4 from the He feed to the compressor while maintaining the maximum return temperature of the UF_4 to the reactor. The temperature of SEP-2 was fixed at 1310 K, just 10 K above the melting point of UF_4, by removal of heat in the cooler, PRICOOL1. A full stream table for the VCR gas recycle loop (utilizing a UF_4 concentration of 30%) is available for review in Appendix B. The temperature of SEP-3 was arbitrarily set at 850 K, a temperature at which UF_4 is solid, by heat removal in PRICOOL2. The model has the UF_4 stream UF_4-3A from SEP-3 being heated to the same temperature as the UF_4 from SEP-2 before being returned to the reactor. In actuality, two heat exchangers would be operated in parallel upstream of SEP-3. The offline heat exchanger would be heated and the product sent to fission product recovery. The temperature at SEP-4 was cooled down to 323 K in order to reduce the energy costs of the He compressor system and reduce trace amounts of UF_4.

The results of a range of UF_4 concentration cases, detailing UF_4 separation from each successive unit's overhead vapor stream, are listed in Table 3. Although a small percentage of UF_4 is evident in vapor stream OVDH-3A from SEP-3, in actuality, the UF_4 has already been removed by condensation on the walls of the upstream parallel heat exchanger. Detailed calculations for all UF_4 separation cases examined are tabulated in Table B-1 of Appendix B. All cases resulted in adequate separation of UF_4 from the He flow at the third separation unit (SEP-3).

TABLE 3
SUMMARY OF UF_4 SEPARATION THROUGH UNITS SEP-1 THROUGH SEP-4

Case	Stream	OVHD-1A	OVHD-2A	OVHD-3A	OVHD-4A
10% UF_4	**Temp, K**	1604	1310	850	323
	Mol% UF_4	4.30E-02	9.58E-03	1.83E-05	0
	Mass% UF_4	5.72E-04	1.23E-04	2.33E-07	0
30% UF_4	**Temp, K**	1627	1310	850	323
	Mol% UF_4	8.96E-02	1.61E-02	3.04E-05	0
	Mass% UF_4	1.25E-03	2.08E-04	3.87E-07	0
60% UF_4	**Temp, K**	1570	1310	850	323
	Mol% UF_4	3.86E-01	6.18E-02	1.17E-04	0
	Mass% UF_4	7.95E-03	8.38E-04	1.49E-06	0

Another process modification required was the addition of interstage cooling to the He Compressor system (MULTICOMP). Without interstage cooling the He Compressor outlet temperature was over 1800 K, too high to cool the walls of the MHD Generator. In between each stage of MULTICOMP (three stages total), the internal stream was reduced in temperature back to the starting value of 323 K. As mentioned earlier, the He stream (OVHD-4A) from SEP-4 eventually leading into the compressor system was cooled to 323 K, in order to reduce the work input needed for the compressors to increase the pressure of the He back up to 60 atm. Work of compression can be simplistically represented by the equation

$$W_s = \frac{n\gamma RT_{init}}{(0.88)(\gamma - 1)}\left[\left(\frac{P_2}{P_1}\right)^{\frac{(\gamma-1)}{n\gamma}} - 1\right]$$

where n = number of stages, γ = ratio of heat capacities, T_{init} = initial temperature, P_2/P_1 = pressure ratio (Green, 1999). The temperature inlet reduction and interstage cooling reduced the required work of compression for the compressors by 50% for all cases considered. In order to regain some of the heat lost during the compression process, a recuperator loop was introduced into the simulation. The heat integration was accomplished by adding a heat exchanger (RECUP) to the He stream (OVHD-3A) before

the temperature was decreased for the compressors. After the He stream passes through the compressor system, the stream is directed through RECUP with an approach temperature of 20 K to the initial temperature of 850 K. The approach temperature is the ΔT between the hot side inlet stream and cold side outlet stream. The smaller the approach temperature, the larger the heat exchanger has to be to achieve it.

Optimization of the simulation consisted of performing a sensitivity analysis to maximize the temperature of the combined UF_4 stream UF_4-ALL returning to the gas core. A sensitivity analysis is a model analysis tool within Aspen Plus. To perform a sensitivity analysis, a flowsheet variable is defined (such as stream temperature), and results of multiple runs are tabulated, through variation of another flowsheet variable within a particular range. The temperature of the stream was maximized by examining the results of varying the outlet temperature of the Ultrasafe Heat Exchanger (PRIMHX) within the liquid temperature range of UF_4. Displayed in Table 4 are the results of the sensitivity analysis for each concentration of UF_4 studied.

TABLE 4
SENSITIVITY AND ANALYSIS RESULTS EXAMINING UF_4 STREAM TEMPERATURE

% Concentration of UF_4	PRIMHX temperature, K	UF_4-ALL max temperature, K
10	1604	1597
20	1627	1604
30	1624	1592
40	1609	1575
50	1591	1556
60	1570	1536

Once the sensitivity analysis was complete, each case was run with the new PRIMHX outlet temperatures to confirm the results, with the gas core inlet stream, VCR-IN, set as close as possible to the combined UF_4 and He outlet stream from the process. For all simulations, the ΔT between streams TO-VCR and VCR-IN varied by less than 0.3%.

4.2.2. UF_4 Concentration Effects

Once adequate separation of UF_4 from the He stream was achieved, further design and analysis work was completed studying the effects of different UF_4 concentrations. As previously mentioned, UF_4 concentrations of 10% to 60% were examined. First

simulations were implemented so as to automatically control set points of key variables in Aspen Plus. The total flowrate through the gas core of the reactor was manipulated to maintain the power at 100 MW while keeping the outlet temperature at 2500 K. The outlet pressure of the MHD Generator was manipulated to maintain an outlet temperature of 1800 K. Table 5 presents the resulting flowrates and pressures for the six UF_4 concentrations examined.

TABLE 5
RESULTS OF VARYING UF_4 CONCENTRATIONS

% Concentration of UF_4, Stream VCR-IN	REACTOR Inlet Flowrate (kmol/s), Stream VCR-IN	MHD Outlet Pressure (atm), Stream HOT-3
10	1.84	14.9
20	1.17	8.72
30	0.857	5.07
40	0.677	2.95
50	0.559	1.72
60	0.476	1.00

Increasing UF_4 concentration decreases both the flowrate into the reactor and the pressure out the MHD generator. These trends are mainly a result of the increased heat capacity of the process stream, due to UF_4 having a more than four times higher heat capacity than He from 1000 K to 3500 K. It should be noted that further simulations with higher concentrations of UF_4 were conducted, but the outlet pressure of the MHD generator dropped to almost zero in attempting to keep the outlet temperature at 1800 K. This fact combined with the results to be discussed next precluded higher UF_4 concentration studies from being included in this report.

The net power output of the MHD system is defined as the net power of the MHD generator (MHD) minus the net power requirements of the He compressor (MULTICOMP). When examined, this net power output was found to be much greater than depicted in Fig. 8. The increased power output stems from two possible sources. One, the He compressor was originally designated in the schematic as a one-stage unit with an inlet temperature of 1000 K. This design, as previously mentioned, is more than 50% more energy “expensive” than a multistage compressor with interstage cooling. Two, the actual thermodynamics of the MHD generator may be slightly different than the isentropic turbine chosen to represent the unit. Figure 9 shows the MHD system net

power, the Ultrasafe Heat Exchanger (PRIMHX) outlet temperature, and the final UF_4 stream temperature, plotted against the % concentration of UF_4 into the reactor.

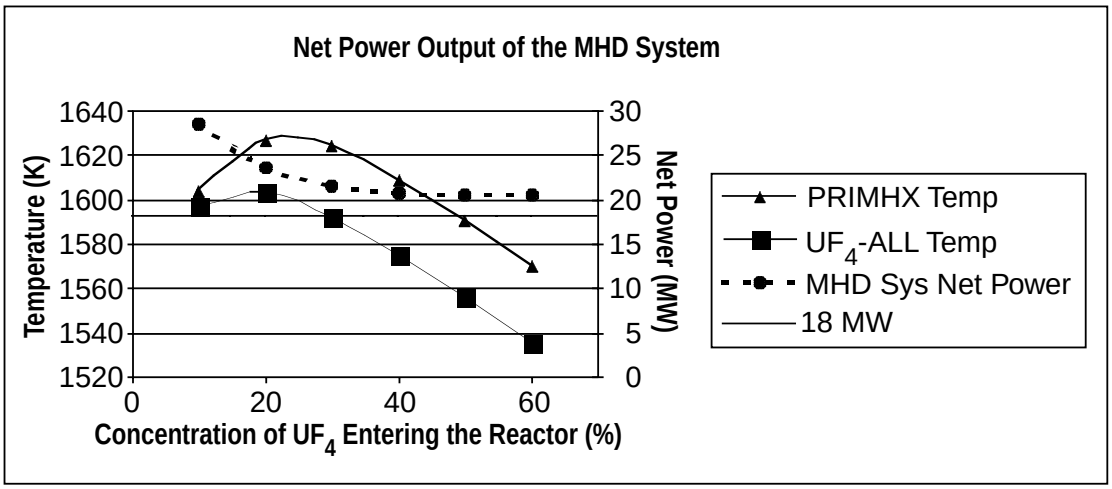

Fig. 9. Examination of the net power versus UF_4 concentration in the gas recycle loop.

Upon analysis of the simulations, it should be noted that the net power of the MHD system is maximum below 10% UF_4, while the Ultrasafe Heat Exchanger (PRIMHX) outlet temperature is maximum slightly above 20%. The UF_4 concentration does have a lower limit since there needs to be enough UF_4 in the reactor stream to reach criticality. The appropriate choice of UF_4 concentration also depends on the thermodynamics of the MHD generator as well as the dominant energy system for power output of the VCR. Reverting to general basic principles, since the MHD generator generates power without being subject to the Carnot limit on efficiency, it seems reasonable that maximizing this unit's power output would be the desirable choice. Since several variables are not known at this time, further discussion of the VCR power output will not be analyzed further in this report.

4.2.3. Fission Products

Once a robust Aspen Plus model simulating UF_4 and He separation was complete, attention turned to fission products in the VCR gas recycle loop. The initial study consisted of UF_4 fission product abundance calculations, literature research of specific compounds for incorporation into the model, and finally, process engineering applied to the separation and removal of fission products from the gas recycle loop.

Table B-3 of Appendix B lists the fractional yield (% amu) of a particular isotope (A) and atomic number (Z) from the fission of UF_4. The yield is expressed as percent per amu, so when the yields are summed they add up to 200%. From the fractional yield,

element yields were tabulated and, when combined with fluorine coordination numbers for those elements, a fluorine requirement number was calculated. Coordination numbers are analogous with oxidation states. In this case, the most stable oxidation state of a particular element, along with fluorine's oxidation state of –1, dictates the number of fluorine atoms (i.e., the coordination number) that will combine with that particular element. The fluorine requirement number represents the fraction of the total fluorine in the system required for each isotope to match its coordination number and form a stable compound. The number is calculated using the equation

$$F_{\text{req}} = \frac{\%yield \times F_{\text{coord}} \times 2}{\%yield\ total} \quad .$$

It should be noted that when the fluorine requirement numbers are summed and scaled, 15% more fluorine atoms are needed than are available to combine with fission products. This will result in a percentage of the fission products not being fluorinated. In Fig. 10, all the elements from the fission process greater than 1% in abundance are charted. It should be noted that thermodynamic data for metal fluorides in gaseous states is very limited, with most fundamental research having been conducted in the early to mid 20th century. Elements depicted with solid bars are the ones chosen for inclusion into the VCR simulation and represent approximately 74% of the total fission products created.

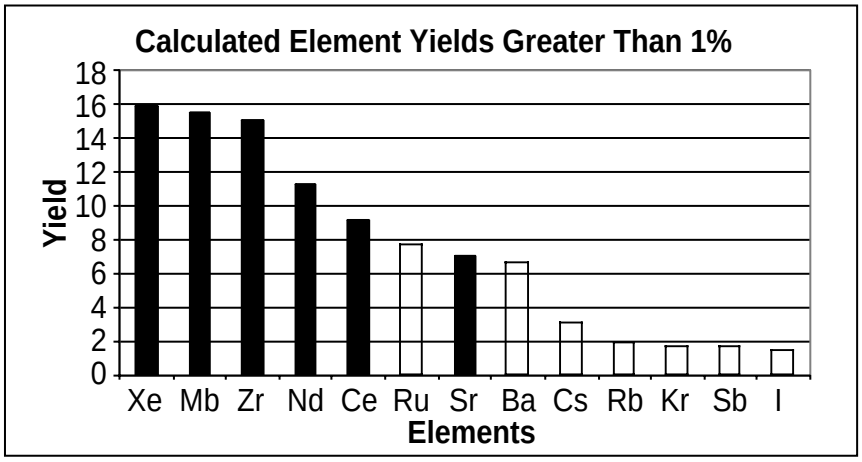

Fig. 10. UF_4 Fission Product Element Yields greater than 1%.

These six particular elements were chosen for a variety of reasons, dominated by the facts that these elements are relatively large in abundance compared to the other species formed and thermodynamic data was available for review. Individually, xenon was a natural choice, as it does not require fluorine. Molybdenum and zirconium were chosen since they form high vapor pressure compounds that cause them to separate with He. Neodymium, cerium, and strontium were chosen for the low vapor pressure compounds

they form, resulting in their separation with UF_4. The overall result is three compounds that will separate with He, and three that go with UF_4. The elements chosen for inclusion, their % yield, coordination number and compound formed are listed in Table 6. In Appendix B, properties used for these compounds are available for review.

TABLE 6
COMPOUNDS CHOSEN FOR INCLUSION
AS FISSION PRODUCTS IN THE VCR SIMULATION

Element	% Yield	Coordination Number	Compound Formed
Xe	15.93	0	Xe
Mo	15.55	6	MoF_6
Zr	15.06	4	ZrF_4
Nd	11.33	3	NdF_3
Ce	9.18	3	CeF_3
Sr	7.09	2	SrF_2
Total %	74.14		

The six chosen fission products were added to the VCR simulation in ppm concentration just after the gas core in stream FISS-IN. The fission product separation through separator units SEP-1 through SEP-4 dominated by vapor pressure characteristics of each compound, and did not vary with UF_4 concentration significantly. As illustrated in Table 7, for a 30% UF_4 simulation the separation was nearly perfect for each compound, and did not require additional process engineering.

Once separation was achieved for the fission products, removal from the gas recycle loop was the next engineering focus point. In order to keep the energy required for removal of the fission products to reasonable values, it was decided that the streams with the largest concentrations of fission products with temperature profiles that would allow for easy fission product removal. For the high vapor pressure fission products, this would be stream OVHD-4A, for the low vapor pressure fission products, stream UF_4-1A. Both these streams had 10% bypass streams split off leading to fission product removal units. The main fission product constituent of stream OVHD-4A is Xe but this stream also contains a significant amount of MoF_6. Unfortunately, Xe's properties are (relatively) so similar to those of He that, in order to apply a standard separator unit to the stream, the temperature would have to be dropped to below the boiling point of liquid Xe (165.03 K

at 1 atm) and a large investment of power would be required to achieve adequate removal. At this time, a particular method has not yet been chosen, and the separation is being carried out without taking into account energy requirements. Other separation techniques such as cryogenic distillation or gas membrane separation are being considered, but this is an area that will require additional process engineering. On the other hand, the ZrF_4 in stream UF_4-4A would actually have been removed in the previously mentioned parallel heat exchanger system in front of SEP-3.

TABLE 7
SEPARATION OF FISSION PRODUCTS FOR A 30% UF_4 SIMULATION

Compound	OVHD-1A	OVHD-2A	OVHD-3A	OVHD-4A
Xe	99.98%	99.99%	100.00%	100.00%
ZrF_4	100.00%	99.99%	91.24%	0.00%
MoF_6	99.95%	99.93%	99.93%	99.93%
NdF_3	0.02%	0.00%	0.00%	0.00%
CeF_3	0.03%	0.00%	0.00%	0.00%
SrF_2	0.00%	0.00%	0.00%	0.00%

The low vapor pressure fission products proved easier to separate and remove from the UF_4 flow since the temperature and pressure values required for separation of the three main fission products (NdF_3, CeF_3, SrF_2) are easily achieved with standard separation units. Initial simulations applied a single flash drum that would vaporize a certain percentage of the incoming liquid UF_4 stream, separating the fission products out the bottom of the unit. A flash drum is a non-adiabatic separator. Heat is manipulated to achieve desired separation, and it is controlled by specifying the outlet pressure or temperature, along with heat duty or percent of the inlet stream to be vaporized. More simulations with dual flash drums were completed next, with the additional variable of UF_4 concentration, in order to study power requirements. In Fig. 11, the results of three test runs at 10%, 35%, and 60% UF_4 concentration are displayed. The two best configurations, with two drums, vaporizing 50% and 80% of the incoming stream respectively, are compared for required power input for vaporization and resulting fission product removed expressed as circulating activity. Circulating activity, simply defined, is the ratio of the total quantity of fission product in the recycle loop over the quantity of product removed with each pass through the loop. A low circulating activity is desirable for safety reasons.

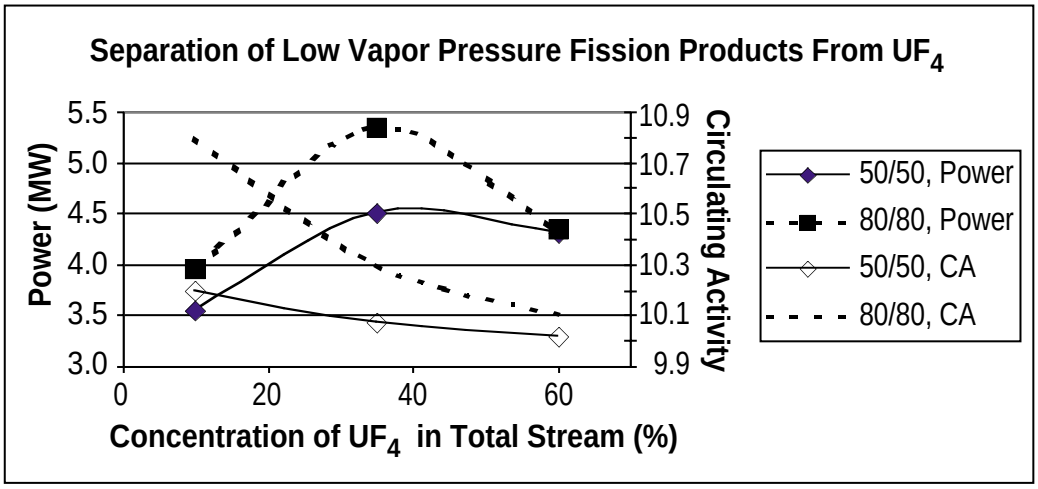

Fig. 11. Separation of low vapor pressure fission products from the UF_4 stream.

Ideally, the goal of fission product separation is a low power requirement, coupled with a low circulating activity in as small a stream of UF_4 as can be reasonably achieved. Individual circulating activities for the fission products will be addressed in the next paragraph, but for Fig. 11, the three circulating activities of NdF_3, CeF_3, and SrF_2 were summed then divided by the total number of species to develop an average circulating activity. As can be seen in the graph, the 50–50 dual separator system has lower power requirements, as well as lower circulating activity for all UF_4 concentrations examined. Additionally, the flowrates of UF_4 through the flash drum system, while dependant upon initial UF_4 concentration, were minimized in a two-unit separator system compared to a single unit.

The circulating activities for the each of the fission products compared with UF_4 concentration are displayed in Fig. 12. The actual circulating activity for the VCR gas recycle loop is unknown, but it is controlled by the rate of fission product generation coupled with the maximum circulating activity allowable from a safety point of view.

Since the removal of Xe, ZrF_4, and MoF_6 is given as a set point, their circulating activities are held constant. The circulating activities of NdF_3, CeF_3, and SrF_2, which were partially controlled by the separation activities in the dual flash drum units FISSEP1 and FISSEP2, varied significantly with the amount of vaporization in these separators and slightly with UF_4 concentration. Generally, under the conditions studied, individual circulating activities of the low vapor pressure fission products varied from a high of 20 utilizing a single flash drum, to a low of 8 for dual units. The choice of dual flash drums vaporizing 50% of the incoming stream, as previously mentioned, had the lowest circulating activity for the lowest power requirement.

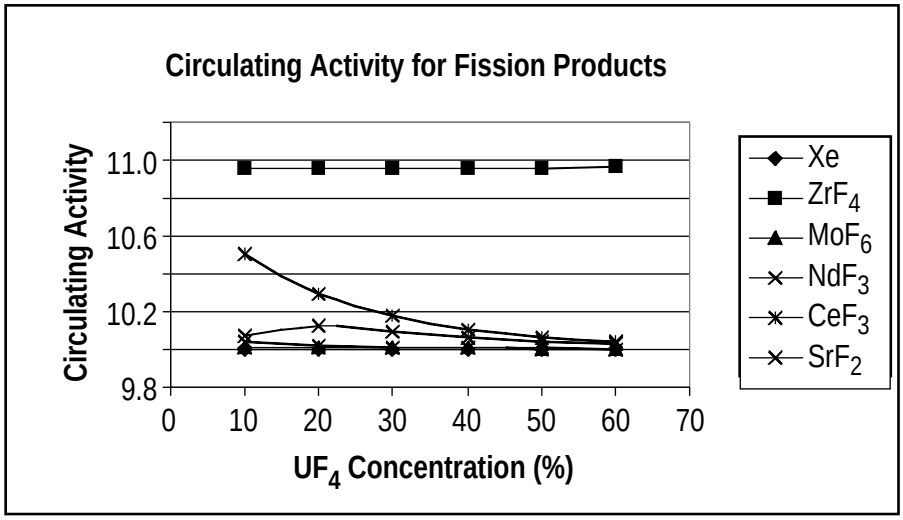

Fig. 12. Circulating activity of the fission products in VCR simulation.

4.3. Future Work

A study of the removal of fission products from the gas recycle stream will be the initial focus of future work on the simulation. As mentioned, cryogenic distillation and gas membrane separation are being considered for high vapor pressure fission product removal. Additionally, for both low and high vapor pressure fission products, absorber/stripper columns utilizing either BeF_2 or "Flibe" (a mixture of two parts LiF and one part BeF_2) will be examined for possible utilization. The final configuration will depend highly upon the maximum allowable circulating activity through the gas recycle loop and the flowrate ratios of UF_4 to He. Further study will also examine fission product decomposition and whether additional species need to be incorporated into the simulation.

Once the systems for fission product separation and removal have been identified, additional process engineering examining heat integration opportunities will be undertaken. This, coupled with possible corrections in the thermodynamics of the MHD generator and He compressor, will have an impact on the final power output and energy efficiency of the entire gas recycle loop.

4.4. Conclusion

The Aspen Plus simulation has facilitated application of process engineering to various aspects of the VCR gas recycle loop. Examination of several parameters such as equipment requirements for UF_4 and He separation, identification and removal of fission products, and overall power outputs will help determine the feasibility of the VCR concept.

Key factors identified for UF_4 and He separations are the necessity for extra separator units, coupled with reductions in stream temperatures, to achieve adequate separation. The use of dual heat exchanger systems for removal of solidified UF_4 and fission products will be necessary as well. With these reduction in stream temperatures, heat integration becomes more important to the overall power output of the VCR and consequently requires the addition of recuperator loops to recapture lost heat.

Fission products, while low in concentration, play a pivotal role by requiring not only additional equipment for separations and removal, but also modifications to the overall system to meet allowable concentration standards for circulating activity. The high vapor pressure fission products (Xe, MoF_6, ZrF_4) will require atypical equipment and procedures to achieve removal, such as cryogenic distillation, while the low vapor pressure products can most likely make use of standard equipment such as flash drums.

Finally, it has been demonstrated that the overall power output of the VCR system can be altered significantly by the gas recycle loop. For example, the application of a multiple stage He compressor with interstage cooling reduced the net power requirement of this particular system by over 50%, although this must be compared to the as yet to be determined thermodynamics of the MHD generator and He compressor. Further heat integration of the UF_4 and He separations and fission product removal systems will most likely alter the VCR power output as well.

APPENDIX A: THERMAL MODEL OF THE REFRIGERATION SYSTEM FOR THE SUPERCONDUCTING COIL OF A DEC FEC REACTOR

An Excel efficiency model for the DEC FEC refrigeration system is presented. The model is relatively simple but should be adequate for preliminary investigations. The model was calibrated by using a large 30 MJ superconducting magnet made by GA in the 1980s. The calculation of this superconducting coil is included in the spreadsheet. This design was used to set one of the adjustable parameters.

The model uses the mass of the coil to calculate the cross sectional area of the coil supports, the primary contribution to the conductive heat load. The length of the supports is somewhat constrained by geometry. They have to be at least as long as the insulation gap, yet short enough to fit within the insulation package.

The radiant heat leakage through the multi-layer insulation (MLI), or "superinsulation", is treated as an equivalent thermal conductivity. The heat transfer from inside the coil bore may be based on a different warm temperature than the outside of the coil. The maximum temperature of the superinsulation is about 500 K. The MLI thickness is assumed to be the same inside the coil bore and outside the coil. The thickness of the insulation layer outside the coil could be increased to increase efficiency. In the case shown in the spreadsheet the layer thickness is optimized. Making the inside layer thicker increases the diameter of the coil and the increase in area results in a decrease in efficiency. We assume that conventional coolants will be used to bring the wall between the reactor and the coil to approximately room temperature. The "knockdown" factor converts the calculated optimal radiant heat leak to a "real world" heat leak. This "fudge" factor was determined from the 30 MJ coil. In a perfect world this factor could be reduced to 1.0.

The miscellaneous leakage factor accounts for heat leaks due to the current leads, liquid cryogen transfer lines, instrumentation wires, AC losses, etc. A more detailed model could give a better estimate of the miscellaneous heat leaks but more design information would be required. The 30 MJ coil did not have a hot shunt and disconnectable current leads so our model does not include this feature. Adding this feature might reduce the miscellaneous leak factor from 1/3 to 1/4. The majority of the miscellaneous leak results from the cryogen transfer lines. Nailing down this factor would require determination of the distance from the cryogenic plant to the coil.

The efficiency of the cryogenic plant comes from "An Update on Estimating the Cost of Cryogenic Refrigeration" by Byrns and Green, which has a graph of refrigerator efficiency vs. refrigerator capacity. We fitted two cases, an average efficiency case and a high efficiency case.

We have added provisions to calculate the effect of adding a liquid nitrogen intermediate heat intercept. It cuts the power requirements by almost a factor of two but requires a liquid nitrogen plant in addition to the liquid helium plant.

Table A-1 compares the cooling requirements for the benchmark 30 MJ coil and two versions of the DEC FEC coil. Table A-2 shows the Spreadsheet used to calculate these cooling requirements.

TABLE A-1
COMPARISON OF SUPERCONDUCTING COIL COOLING REQUIREMENTS

(**Boldface parameters** can be changed as part of design effort. *Italic parameters* modify the basic efficiency assumptions)	Benchmark 30 MJ Coil	DEC FEC Coil With Single-Stage Cooling	DEC FEC Coil With Two-Stage Cooling	
	30 MJ Coil	DEC FEC Coil	DEC FEC Coil N_2	DEC FEC Coil He
Design Data				
Central magnetic field (T)	**3.92**	**2.5**		
Inside radius— warm (m)	**1.02**	**3**		
Solenoid length — cold (m)	**0.86**	**5**		
Coil temp (K)	**4.2**	**4.2**		
Pack current density (A/m^2)	**15700000**	**30000000**		
G-10 support length (m)	**0.25**	**1.5**		
Inside warm wall temp (K)	**300**	**300**		
Outside warm wall temp (K)	**300**	**300**		
Environment temp (K)	**300**	**300**		
Insulation thickness (m)	**0.1**	**0.5**	**0.35**	0.15
Constants				
Permeability constant (H/m)	1.26E-06	1.26E-06		
Effective thermal conductivity of superinsulation (w/m*K)	*0.00003*	*0.00003*	*0.00003*	*0.00003*
Knockdown factor for real world performance	*3*	*3*	*3*	*3*
Misc heat leak factor	*0.333*	*0.333*	*0.333*	*0.333*
Calculated Results				
Maximum G10 support length	0.97	5.52		
Ratio of support length to solenoid length	0.29	0.30		
Ratio of Insulation thickness to solenoid length	*0.1162791*	*0.1*		
Ratio of average coil diameter to solenoid length	*1.4175349*	*0.70661376*		
Current density (amp-turns)	2.68E+06	9.92E+06		
Pack area (m^2)	1.70E-01	3.31E-01		
Inside radius — cold (m)	1.12	3.50	3.35	3.50
Pack width (m)	0.20	0.07		
Outside radius — cold (m)	1.32	3.57	3.72	3.57
Outside radius warm (m)	1.42	4.07	4.07	3.72
Inside radiation heat leak	1.54	5.43	1.01	4.70
Outside radiation heat leak	1.97	6.37	2.01	5.00
Top/bottom radiation heat leak	2.70	2.31	4.15	0.87
Radiation heat leak (W)	6.20	14.11	7.18	10.57
Pack volume (m^3)	1.31	7.34		
Pack weight (N)	1.14E+05	6.41E+05		

TABLE A-1 (Continued)

(**Boldface parameters** can be changed as part of design effort. *Italic parameters* modify the basic efficiency assumptions)	Benchmark 30 MJ Coil	DEC FEC Coil With Single-Stage Cooling	DEC FEC Coil With Two-Stage Cooling	
	30 MJ Coil	DEC FEC Coil	DEC FEC Coil N_2	DEC FEC Coil He
Calculated Results (continued)				
Maximum G10 support length	0.97	5.52		
Ratio of support length to solenoid length	0.29	0.30		
Ratio of Insulation thickness to solenoid length	*0.1162791*	*0.1*		
Ratio of average coil diameter to solenoid length	*1.4175349*	*0.70661376*		
Current density (amp-turns)	2.68E+06	9.92E+06		
Pack area (m^2)	1.70E-01	3.31E-01		
Inside radius — cold (m)	1.12	3.50	3.35	3.50
Pack width (m)	0.20	0.07		
Outside radius — cold (m)	1.32	3.57	3.72	3.57
Outside radius warm (m)	1.42	4.07	4.07	3.72
Inside radiation heat leak	1.54	5.43	1.01	4.70
Outside radiation heat leak	1.97	6.37	2.01	5.00
Top/bottom radiation heat leak	2.70	2.31	4.15	0.87
Radiation heat leak (W)	6.20	14.11	7.18	10.57
Pack volume (m^3)	1.31	7.34		
Pack weight (N)	1.14E+05	6.41E+05		
Pack weight (kg)	1.17E+04	6.56E+04		
G-10 cross section area (m^2)	4.40E-03	2.48E-02		
G-10 Cross section area (cm^2)	4.40E+01	2.48E+02		
Conduction heat leak (W)	1.56	1.47	0.38	1.20
Rad + conduction heat leak (W)	7.77	15.58	7.55	11.77
Misc heat leak (W)	2.59	5.19	0.56	3.92
Total heat leak (W)	10.36	20.77	8.11	15.69
Carnot ratio	70.43	70.43	2.90	70.43
Reversible power required (W)	729.30	1462.97	23.49	1105.22
Percent Carnot (avg efficiency) (%)	5.32	6.64	4.88	6.09
Power required (avg efficiency) (W)	13,717	22,028	481	18,141
Power requirement for two stage cooling (avg efficiency) (W)				18,622
Percent Carnot (high efficiency) (%)	8.63	10.81	7.92	9.91
Power required (high efficiency) (W)	8,447	13,528	297	11,152
Power requirement for two stage cooling (high efficiency) (W)				11,448

TABLE A-2
SPREADSHEET FOR SUPERCONDUCTING COIL COOLING REQUIREMENTS

	A	B
1	(**Boldface parameters** can be changed as part of design effort. *Italic parameters* modify the basic efficiency assumptions)	DEC FEC cooling requirements for single stage cooling
2		
3		DEC FEC Coil
4	**Design Data**	
5	Central magnetic field (Tesla)	**2.5**
6	Inside radius — warm (meter)	**3**
7	Solenoid length — cold (meter)	**5**
8	Coil temp (K)	**4.2**
9	Pack current density (A/m^2)	**30000000**
10	G-10 support length (m)	**1.5**
11	Inside warm wall temp (K)	**300**
12	Outside warm wall temp (K)	**300**
13	Environment temp (K)	**300**
14	Insulation thickness (m)	**0.5**
15		
16	**Constants**	
17	Permeability constant (H/m)	0.00000126
18	Effective thermal conductivity of superinsulation(w/m*K) Use effective thermal conductivity of 0.03mW/m*K (MLI + good vacuum) see Cryogenic Process Engineering by Timmerhaus pg 389.	*0.00003*
19	Knockdown factor for real world performance Value determined from 30 mJ coil. This is one of the largest solenoids every built in terms of both size and stored energy.	*3*
20	Misc heat leak factor. Accounts for heat leak due to current leads, liquid cryogen transfer lines, instrumentation wires, AC losses, etc	*=1/3*
21		
22	**Calculated results**	
		=(B7^2+2*B7*B14+2*B14
23	Maximum G10 support length	^2)^0.5
24	Ratio of support length to Solenoid length	=B10/B7
25	Ratio of Insulation thickness to solenoid length	*=B14/B7*
26	Ratio of average coil diameter to solenoid length	*=0.5*(B29+B31)/B7*
27	Current density (amp-turns)	=(B5*B7)/B17
28	Pack area (m^2)	=B27/B9
29	Inside radius — cold (m)	=B6+B14
30	Pack width (m)	=B28/B7
31	Outside radius — cold (m)	=B29+B30
32	Outside radius warm (m)	=B31+B14
33	Inside radiation heat leak	=B19*2*PI()*B7*B18*(B11–B8)/LN((B29)/(B6))
34	Outside radiation heat leak	=B19*2*PI()*B7*B18*(B12-B8)/LN((B32)/(B31))
35	Top/bottom radiation heat leak	=B19*2*2*PI()*2*PI()*[0.5*(B29+B31)]*B18*(0.5*B11+0.5*B12-B8)/LN[(PI()*B14+B30)/(B30)]

TABLE A-2 (Continued)

	A	B
	Calculated results (continued)	
36	Radiation heat leak (W)	=SUM(B33:B35)
37	Pack Volume (m^3)	=PI()*B7*[(B31^2)-(B29^2)]
38	Pack weight (N) assume the coil pack has the same density as copper = 87.3 N/m^3	=B37*87300
39	Pack weight (kg) same as above except in kg: density = 8940kg/m^3	=B37*8940
40	G-10 Cross section area (m^2) Assume struts made of G-10 composite material [strength = 60 ksi (414 MPa)]/ Use 1/4 strength + factor of safety of 2 + assume same area of straps holding coil down (earthquake)	=(B38/[414000000/(4*2*2)])
41	G-10 Cross section area (cm^2)	=B40*10000
42	Conduction heat leak (W) G-10 thermal conductivity (k) varies greatly with temperature. However to simplify, use k at 77 K: 0.30 W/m K	=[0.3*B40*(B11-B8)]/B10
43	Rad + conduction heat leak (W)	=B36+B42
44	Misc heat leak (W) includes heat leak due to current leads, liquid cryogen transfer lines, instrumentation wires, AC losses, etc	=B43*B20
45	Total heat leak (W)	=B43+B44
46	Carnot ratio. This is the ratio between the net input power and the refrigeration produced	=(B13-B8)/B8
47	Reversible power required (W)	=B45*B46
48	Percent Carnot (avg efficiency) (%)	= –1.06 + 55.6*EXP[–1.19* (B45/1000)^-0.131]
49	Power required (avg efficiency) (W)	=B47/(B48/100)
50	Power requirement for two stage cooling (avg efficiency) (W)	
51	Percent Carnot (high efficiency) (%)	= –1.86 + 91.5*EXP[–1.19* (B45/1000)^–0.131]
52	Power required (high efficiency) (W)	=IF[B10<B23,B47/(B51/100), “Support is too long”]

APPENDIX B: MODEL OF THE GAS RECYCLE LOOP OF THE VAPOR CORE REACTOR

B.1. Properties of UF_4

MW = 314.0225 V_{crit} = 162.5 cc/mol

T_{nbp} = 1723 K[1] V_b = 56.281 cc/mol

T_{mp} = 1309 K Z_{crit} = 0.1707

T_{crit} = 2415 K[2]

P_{crit} = 208.2 atm

Extended Antoine's Equation

$$\ln P(atm) = 74.217 - \frac{37977}{T\,(K)} - 7.0 \ln T,\ (T \le 1600\,K)^{3} \quad .$$

Extended Antoine's Equation adapted to Aspen Plus

$$\ln P(atm) = 74.217 - \frac{-37977}{T\,(K)} - 7.0 \ln T,\ (T \le 1600\ K) \quad ,\ (1000\text{–}2500\ K),$$

Aspen Plus extrapolates ln *P* vs. 1/T outside this range.

Liquid Density

$$\rho\left(kg/m^3\right) = 7.784 \times 10^3 - 0.992\,T,\ (1300 - 1700\,K) \quad .$$

B.2. Modeling of the Gas Recycle Loop

(Starts next page)

[1]Adapted from (Winter, 2001).
[2] All critical properties of UF_4 and fission products estimated with a critical property estimation method (Hakuta, 1970).
[3] Extended Antoine's and density equations adapted from (Anghaie, 1992).

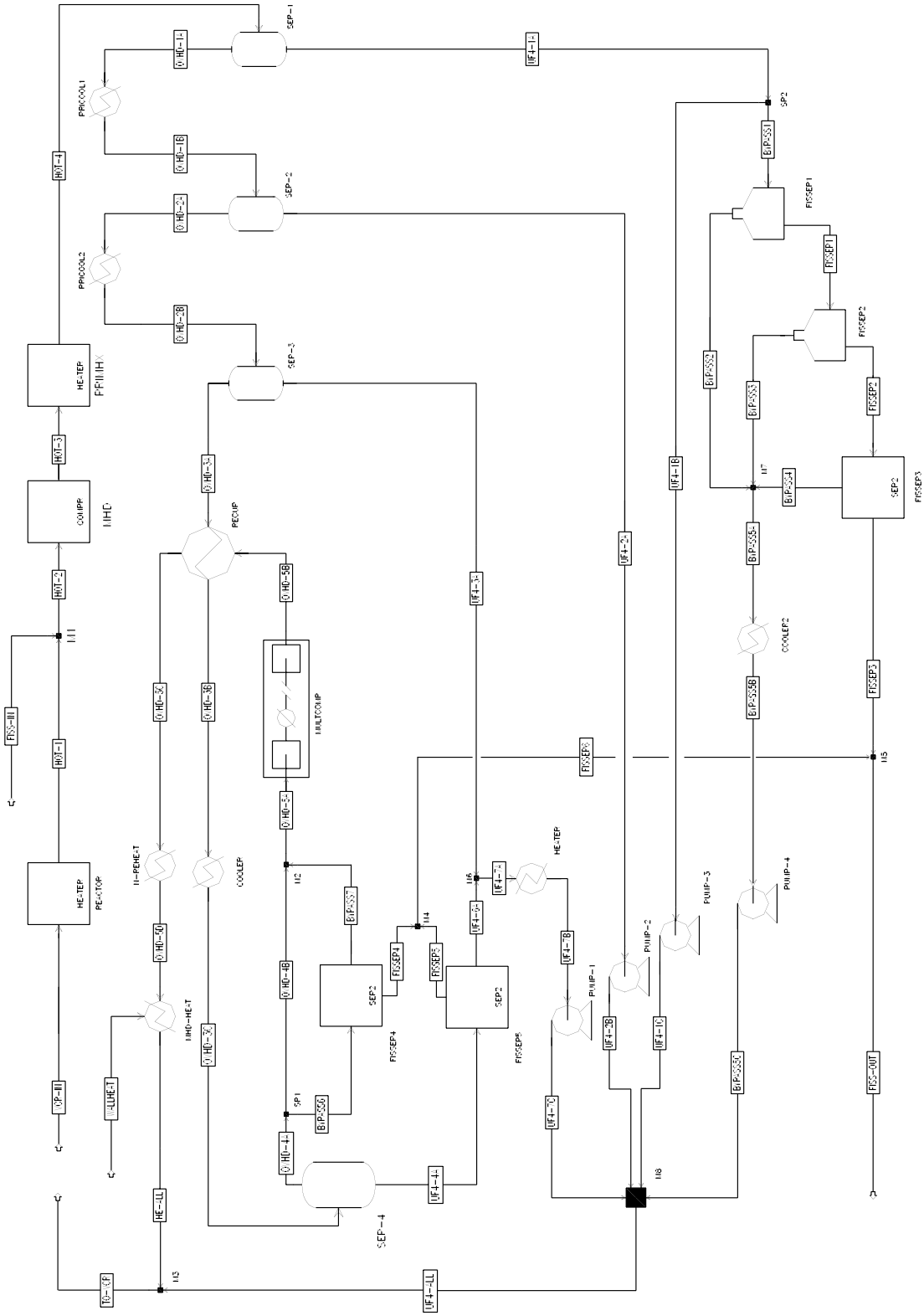

Fig. B–1. Process flow diagram (PFD) of the vapor core reactor gas recycle loop.

TABLE B–1
STREAM TABLE FOR VCR GAS RECYCLE LOOP

Stream	**BYPASS1**	**BYPASS2**	**BYPASS3**	**BYPASS4**	**BYPASS5A**	**BYPASS5B**	**BYPASS5C**
Mole flow, kmol/s							
He	0.0E+00	0.0E+00	0.0E+00	0.0E+00	0.0E+00	0.0E+00	0.0E+00
UF_4	2.0596E-02	1.0298E-02	5.1490E-03	5.1487E-03	2.0596E-02	2.0596E-02	2.0596E-02
Xe	0.0E+00	0.0E+00	0.0E+00	0.0E+00	0.0E+00	0.0E+00	0.0E+00
ZrF_4	3.0826E-13	3.0826E-13	0.0E+00	0.0E+00	3.0826E-13	3.0826E-13	3.0826E-13
MoF_6	4.9800E-11	4.9743E-11	5.6906E-14	0.0E+00	4.9800E-11	4.9800E-11	4.9800E-11
NdF_3	9.9580E-08	4.4690E-10	4.4492E-10	0.0E+00	8.9182E-10	8.9182E-10	8.9182E-10
CeF_3	9.9575E-08	8.4559E-10	8.3846E-10	0.0E+00	1.6841E-09	1.6841E-09	1.6841E-09
SrF_2	9.9598E-08	6.9481E-11	6.9437E-11	0.0E+00	1.3892E-10	1.3892E-10	1.3892E-10
Total flow, kmol/s	2.0596E-02	1.0298E-02	5.1490E-03	5.1487E-03	2.0596E-02	2.0596E-02	2.0596E-02
Total flow, kg/s	6.4676E+00	3.2338E+00	1.6169E+00	1.6168E+00	6.4675E+00	6.4675E+00	6.4675E+00
Temperature, K	1.6240E+03	1.9361E+03	1.9361E+03	1.9361E+03	1.9361E+03	1.9361E+03	1.9402E+03
Pressure, atm	5.0683E+00	5.0683E+00	5.0683E+00	5.0683E+00	5.0683E+00	5.0683E+00	6.0000E+01
Vapor frac	0.0	1.0	1.0	1.0	1.0	0.0	0.0
Liquid frac	1.0	0.0	0.0	0.0	0.0	1.0	1.0

Stream	**BYPASS6**	**BYPASS7**	**FISS-IN**	**FISS-OUT**	**FISSEP1**	**FISSEP2**	**FISSEP3**
Mole flow, kmol/s							
He	6.0024E-02	6.0024E-02	0.0E+00	0.0E+00	0.0E+00	0.0E+00	0.0E+00
UF_4	0.0000E+00	0.0E+00	0.0E+00	0.0E+00	1.0298E-02	5.1487E-03	0.0E+00
Xe	9.9600E-08	0.0E+00	9.9600E-07	9.9600E-08	0.0E+00	0.0E+00	0.0E+00
ZrF_4	0.0E+00	0.0E+00	9.9600E-07	9.0873E-08	0.0E+00	0.0E+00	0.0E+00
MoF_6	1.0193E-07	0.0E+00	1.0200E-06	1.0193E-07	5.6972E-14	0.0E+00	0.0E+00
NdF_3	0.0E+00	0.0E+00	9.9600E-07	9.8689E-08	9.9134E-08	9.8689E-08	9.8689E-08
CeF_3	0.0E+00	0.0E+00	9.9600E-07	9.7891E-08	9.8729E-08	9.7891E-08	9.7891E-08
SrF_2	0.0E+00	0.0E+00	9.9600E-07	9.9459E-08	9.9529E-08	9.9459E-08	9.9459E-08
Total flow, kmol/s	6.0024E-02	6.0024E-02	6.0000E-06	5.8844E-07	1.0298E-02	5.1490E-03	2.9604E-07
Total flow, kg/s	2.4028E-01	2.4025E-01	1.0333E-03	1.0132E-04	3.2338E+00	1.6169E+00	5.1649E-05
Temperature, K	3.2300E+02	3.2300E+02	2.5000E+03	1.4449E+03	1.9361E+03	1.9361E+03	1.9361E+03
Pressure, atm	5.0683E+00	5.0683E+00	6.0000E+01	5.0683E+00	5.0683E+00	5.0683E+00	5.0683E+00
Vapor frac	1.0	1.0	0.5	0.5	0.0	0.0	0.0
Liquid frac	0.0	0.0	0.5	0.5	1.0	1.0	1.0

TABLE B–1 (Continued)

Stream	FISSEP4	FISSEP5	FISSEP6	HE-ALL	HOT-1	HOT-2	HOT-3
Mole flow, kmol/s							
He	0.0E+00	0.0E+00	0.0E+00	6.0024E-01	6.0024E-01	6.0024E-01	6.0024E-01
UF_4	0.0E+00	0.0E+00	0.0E+00	0.0E+00	2.5724E-01	2.5724E-01	2.5724E-01
Xe	9.9600E-08	0.0E+00	9.9600E-08	8.9640E-07	0.0E+00	9.9600E-07	9.9600E-07
ZrF_4	0.0E+00	9.0873E-08	9.0873E-08	0.0000E+00	0.0E+00	9.9600E-07	9.9600E-07
MoF_6	1.0193E-07	4.4332E-12	1.0193E-07	9.1735E-07	0.0E+00	1.0200E-06	1.0200E-06
NdF_3	0.0E+00	0.0E+00	0.0E+00	0.0E+00	0.0E+00	9.9600E-07	9.9600E-07
CeF_3	0.0E+00	0.0E+00	0.0E+00	0.0E+00	0.0E+00	9.9600E-07	9.9600E-07
SrF_2	0.0E+00	0.0E+00	0.0E+00	0.0E+00	0.0E+00	9.9600E-07	9.9600E-07
Total flow, kmol/s	2.0153E-07	9.0878E-08	2.9241E-07	6.0024E-01	8.5748E-01	8.5748E-01	8.5748E-01
Total flow, kg/s	3.4474E-05	1.5197E-05	4.9671E-05	2.4028E+00	8.3183E+01	8.3184E+01	8.3184E+01
Temperature, K	3.2300E+02	3.2300E+02	3.4248E+02	1.5500E+03	2.5000E+03	2.5000E+03	1.8000E+03
Pressure, atm	5.0683E+00	5.0683E+00	5.0683E+00	6.0000E+01	6.0000E+01	6.0000E+01	5.0683E+00
Vapor frac	0.7	0.0	0.4	1.0	1.0	1.0	1.0
Liquid frac	0.3	1.0	0.6	0.0	0.0	0.0	0.0

Stream	HOT-4	OVHD-1A	OVHD-1B	OVHD-2A	OVHD-2B	OVHD-3A	OVHD-3B
Mole flow, kmol/s							
He	6.0024E-01	6.0024E-01	6.0024E-01	6.0024E-01	6.0024E-01	6.0024E-01	6.0024E-01
UF_4	2.5724E-01	5.1286E-02	5.1286E-02	7.8337E-04	7.8337E-04	2.7370E-09	2.7370E-09
Xe	9.9600E-07	9.9600E-07	9.9600E-07	9.9600E-07	9.9600E-07	9.9600E-07	9.9600E-07
ZrF_4	9.9600E-07	9.9600E-07	9.9600E-07	9.9595E-07	9.9595E-07	9.0873E-07	9.0873E-07
MoF_6	1.0200E-06	1.0195E-06	1.0195E-06	1.0193E-06	1.0193E-06	1.0193E-06	1.0193E-06
NdF_3	9.9600E-07	1.9568E-10	1.9568E-10	0.0E+00	0.0E+00	0.0E+00	0.0E+00
CeF_3	9.9600E-07	2.5028E-10	2.5028E-10	0.0E+00	0.0E+00	0.0E+00	0.0E+00
SrF_2	9.9600E-07	1.9716E-11	1.9716E-11	0.0E+00	0.0E+00	0.0E+00	0.0E+00
Total flow, kmol/s	8.5748E-01	6.5152E-01	6.5152E-01	6.0102E-01	6.0102E-01	6.0024E-01	6.0024E-01
Total flow, kg/s	8.3184E+01	1.8508E+01	1.8508E+01	2.6490E+00	2.6490E+00	2.4030E+00	2.4030E+00
Temperature, K	1.6240E+03	1.6240E+03	1.3100E+03	1.3100E+03	8.5000E+02	8.5000E+02	3.4302E+02
Pressure, atm	5.0683E+00	5.0683E+00	5.0683E+00	5.0683E+00	5.0683E+00	5.0683E+00	5.0683E+00
Vapor frac	0.8	1.0	0.9	1.0	1.0	1.0	1.0
Liquid frac	0.2	0.0	0.1	0.0	0.0	0.0	0.0

TABLE B–1 (Continued)

Stream	OVHD-3C	OVHD-4A	OVHD-4B	OVHD-5A	OVHD-5B	OVHD-5C	OVHD-5D
Mole flow, kmol/s							
He	6.0024E-01	6.0024E-01	5.4021E-01	6.0024E-01	6.0024E-01	6.0024E-01	6.0024E-01
UF_4	2.7370E-09	0.0E+00	0.0E+00	0.0E+00	0.0E+00	0.0E+00	0.0E+00
Xe	9.9600E-07	9.9600E-07	8.9640E-07	8.9640E-07	8.9640E-07	8.9640E-07	8.9640E-07
ZrF_4	9.0873E-07	0.0E+00	0.0E+00	0.0E+00	0.0E+00	0.0E+00	0.0E+00
MoF_6	1.0193E-06	1.0193E-06	9.1735E-07	9.1735E-07	9.1735E-07	9.1735E-07	9.1735E-07
NdF_3	0.0E+00	0.0E+00	0.0E+00	0.0E+00	0.0E+00	0.0E+00	0.0E+00
CeF_3	0.0E+00	0.0E+00	0.0E+00	0.0E+00	0.0E+00	0.0E+00	0.0E+00
SrF_2	0.0E+00	0.0E+00	0.0E+00	0.0E+00	0.0E+00	0.0E+00	0.0E+00
Total flow, kmol/s	6.0024E-01	6.0024E-01	5.4021E-01	6.0024E-01	6.0024E-01	6.0024E-01	6.0024E-01
Total flow, kg/s	2.4030E+00	2.4028E+00	2.1626E+00	2.4028E+00	2.4028E+00	2.4028E+00	2.4028E+00
Temperature, K	3.2300E+02	3.2300E+02	3.2300E+02	3.2300E+02	3.2300E+02	8.3000E+02	1.4000E+03
Pressure, atm	5.0683E+00	5.0683E+00	5.0683E+00	5.0683E+00	6.0000E+01	6.0000E+01	6.0000E+01
Vapor frac	1.0	1.0	1.0	1.0	1.0	1.0	1.0
Liquid frac	0.0	0.0	0.0	0.0	0.0	0.0	0.0

Stream	TO-VCR	VCR-IN	UF4-1A	UF4-1B	UF4-1C	UF4-2A	UF4-2B
Mole flow, kmol/s							
He	6.0024E-01	6.0024E-01	0.0E+00	0.0E+00	0.0E+00	0.0E+00	0.0E+00
UF_4	2.5724E-01	2.5724E-01	2.0596E-01	1.8536E-01	1.8536E-01	5.0502E-02	5.0502E-02
Xe	8.9640E-07	0.0E+00	0.0E+00	0.0E+00	0.0E+00	0.0E+00	0.0E+00
ZrF_4	9.0513E-07	0.0E+00	3.0826E-12	2.7743E-12	2.7743E-12	4.7382E-11	4.7382E-11
MoF_6	9.1807E-07	0.0E+00	4.9800E-10	4.4820E-10	4.4820E-10	2.0576E-10	2.0576E-10
NdF_3	8.9731E-07	0.0E+00	9.9580E-07	8.9622E-07	8.9622E-07	1.9568E-10	1.9568E-10
CeF_3	8.9811E-07	0.0E+00	9.9575E-07	8.9618E-07	8.9618E-07	2.5028E-10	2.5028E-10
SrF_2	8.9654E-07	0.0E+00	9.9598E-07	8.9638E-07	8.9638E-07	1.9716E-11	1.9716E-11
Total flow, kmol/s	8.5748E-01	8.5748E-01	2.0596E-01	1.8536E-01	1.8536E-01	5.0502E-02	5.0502E-02
Total flow, kg/s	8.3184E+01	8.3183E+01	6.4676E+01	5.8208E+01	5.8208E+01	1.5859E+01	1.5859E+01
Temperature, K	1.5769E+03	1.5100E+03	1.6240E+03	1.6240E+03	1.6253E+03	1.3100E+03	1.3113E+03
Pressure, atm	6.0000E+01	6.0000E+01	5.0683E+00	5.0683E+00	6.0000E+01	5.0683E+00	6.0000E+01
Vapor frac	0.7	0.7	0.0	0.0	0.0	0.0	0.0
Liquid frac	0.3	0.3	1.0	1.0	1.0	1.0	1.0

TABLE B–1 (Continued)

Stream	UF4-3A	UF4-4A	UF4-6A	UF4-7A	UF4-7B	UF4-7C	UF4-ALL
Mole flow, kmol/s							
He	0.0E+00	0.0E+00	0.0E+00	0.0E+00	0.0E+00	0.0E+00	0.0E+00
UF_4	7.8337E-04	2.7370E-09	2.7370E-09	7.8337E-04	7.8337E-04	7.8337E-04	2.5724E-01
Xe	0.0E+00	0.0E+00	0.0E+00	0.0E+00	0.0E+00	0.0E+00	0.0E+00
ZrF_4	8.7216E-08	9.0873E-07	8.1786E-07	9.0508E-07	9.0508E-07	9.0508E-07	9.0513E-07
MoF_6	1.0998E-11	4.4332E-12	0.0000E+00	1.0998E-11	1.0998E-11	1.0998E-11	7.1476E-10
NdF_3	0.0E+00	0.0E+00	0.0E+00	0.0E+00	0.0E+00	0.0E+00	8.9731E-07
CeF_3	0.0E+00	0.0E+00	0.0E+00	0.0E+00	0.0E+00	0.0E+00	8.9811E-07
SrF_2	0.0E+00	0.0E+00	0.0E+00	0.0E+00	0.0E+00	0.0E+00	8.9654E-07
Total flow, kmol/s	7.8346E-04	9.1148E-07	8.2060E-07	7.8428E-04	7.8428E-04	7.8428E-04	2.5725E-01
Total flow, kg/s	2.4601E-01	1.5282E-04	1.3762E-04	2.4615E-01	2.4615E-01	2.4615E-01	8.0781E+01
Temperature, K	8.5000E+02	3.2300E+02	3.2300E+02	8.4945E+02	1.3100E+03	1.3112E+03	1.5929E+03
Pressure, atm	5.0683E+00	5.0683E+00	5.0683E+00	5.0683E+00	1.0360E+01	6.0000E+01	6.0000E+01
Vapor frac	0.0	0.0	0.0	0.0	0.0	0.0	0.0
Liquid frac	1.0	1.0	1.0	1.0	1.0	1.0	1.0

TABLE B–2
UF_4 SEPARATION CALCULATIONS

	10% Case				20% Case			
Stream	**OVHD-1A**	**OVHD-2A**	**OVHD-3A**	**OVHD-4A**	**OVHD-1A**	**OVHD-2A**	**OVHD-3A**	**OVHD-4A**
He, kmol/s	1.6539E+00	1.6545E+00	1.6547E+00	1.6547E+00	9.3498E-01	9.3545E-01	9.3561E-01	9.3561E-01
UF_4, kmol/s	3.6699E-02	7.2994E-04	2.5524E-09	0.0000E+00	4.6230E-02	7.0829E-04	2.4760E-09	0.0000E+00
Mol % He in stream	9.7829E+01	9.9956E+01	1.0000E+02	1.0000E+02	9.5288E+01	9.9924E+01	1.0000E+02	1.0000E+02
Mol % UF_4 in stream	2.1708E+00	4.4098E-02	1.5425E-07	0.0000E+00	4.7116E+00	7.5659E-02	2.6464E-07	0.0000E+00
He, kg/s	6.6204E+00	6.6230E+00	6.6239E+00	6.6239E+00	3.7427E+00	3.7446E+00	3.7452E+00	3.7452E+00
UF_4, kg/s	1.1524E+01	2.2920E-01	8.0145E-07	0.0000E+00	1.4516E+01	2.2240E-01	7.7746E-07	0.0000E+00
Mass % He in stream	3.6488E+01	9.6655E+01	1.0000E+02	1.0000E+02	2.0498E+01	9.4394E+01	1.0000E+02	1.0000E+02
Mass % UF_4 in stream	6.3512E+01	3.3449E+00	1.2099E-05	0.0000E+00	7.9502E+01	5.6063E+00	2.0759E-05	0.0000E+00

	30% Case				40% Case			
Stream	**OVHD-1A**	**OVHD-2A**	**OVHD-3A**	**OVHD-4A**	**OVHD-1A**	**OVHD-2A**	**OVHD-3A**	**OVHD-4A**
He, kmol/s	5.9984E-01	6.0013E-01	6.0023E-01	6.0023E-01	4.0590E-01	4.0607E-01	4.0613E-01	4.0613E-01
UF_4, kmol/s	5.1287E-02	7.8336E-04	2.7370E-09	0.0000E+00	5.3299E-02	9.1115E-04	3.1804E-09	0.0000E+00
Mol % He in stream	9.2123E+01	9.9870E+01	1.0000E+02	1.0000E+02	8.8393E+01	9.9776E+01	1.0000E+02	1.0000E+02
Mol % UF_4 in stream	7.8767E+00	1.3036E-01	4.5599E-07	0.0000E+00	1.1607E+01	2.2388E-01	7.8310E-07	0.0000E+00
He, kg/s	2.4012E+00	2.4023E+00	2.4027E+00	2.4027E+00	1.6248E+00	1.6255E+00	1.6257E+00	1.6257E+00
UF_4, kg/s	1.6104E+01	2.4598E-01	8.5942E-07	0.0000E+00	1.6736E+01	2.8610E-01	9.9865E-07	0.0000E+00
Mass % He in stream	1.2975E+01	9.0712E+01	1.0000E+02	1.0000E+02	8.8494E+00	8.5033E+01	1.0000E+02	1.0000E+02
Mass % UF_4 in stream	8.7025E+01	9.2881E+00	3.5768E-05	0.0000E+00	9.1151E+01	1.4967E+01	6.1427E-05	0.0000E+00

	50% Case				60% Case			
Stream	**OVHD-1A**	**OVHD-2A**	**OVHD-3A**	**OVHD-4A**	**OVHD-1A**	**OVHD-2A**	**OVHD-3A**	**OVHD-4A**
He, kmol/s	2.7943E-01	2.7952E-01	2.7956E-01	2.7956E-01	1.9043E-01	1.9048E-01	1.9050E-01	1.9050E-01
UF_4, kmol/s	5.5241E-02	1.0785E-03	3.7585E-09	0.0000E+00	5.5584E-02	1.2650E-03	4.3961E-09	0.0000E+00
Mol % He in stream	8.3494E+01	9.9616E+01	1.0000E+02	1.0000E+02	7.7406E+01	9.9340E+01	1.0000E+02	1.0000E+02
Mol % UF_4 in stream	1.6506E+01	3.8435E-01	1.3444E-06	0.0000E+00	2.2594E+01	6.5970E-01	2.3076E-06	0.0000E+00
He, kg/s	1.1186E+00	1.1189E+00	1.1191E+00	1.1191E+00	7.6230E-01	7.6250E-01	7.6259E-01	7.6259E-01
UF_4, kg/s	1.7346E+01	3.3865E-01	1.1802E-06	0.0000E+00	1.7453E+01	3.9720E-01	1.3804E-06	0.0000E+00
Mass % He in stream	6.0579E+00	7.6766E+01	1.0000E+02	1.0000E+02	4.1848E+00	6.5750E+01	1.0000E+02	1.0000E+02
Mass % UF_4 in stream	9.3942E+01	2.3234E+01	1.0546E-04	0.0000E+00	9.5815E+01	3.4250E+01	1.8101E-04	0.0000E+00

TABLE B–3
TABULATED FISSION FRAGMENT CALCULATIONS[4]

A (amu)[5,6]	Z (e)	Yield (%/amu)	Isotope Symbol	Element Symbol	Element Yield[7]	Fluorine Coordination No.	Fluorine Requirement
134	54	7.89	Xe-134	Xe	31.72	0	0
138	56	6.69	Ba-138	Ba	13.15	2	0.13436096
133	54	6.67	Xe-133	Xe	31.72	0	0
139	56	6.46	Ba-139	Ba	13.15	2	0.12974167
136	54	6.44	Xe-136	Xe	31.72	0	0
94	40	6.42	Zr-94	Zr	30	4	0.25787663
100	42	6.42	Mo-100	Mo	30.98	3	0.19340748
135	54	6.41	Xe-135	Xe	31.72	0	0
95	42	6.39	Mo-95	Mo	30.98	3	0.1925037
93	40	6.37	Zr-93	Zr	30	4	0.25586825
140	58	6.32	Ce-140	Ce	18.28	3	0.1903949
96	40	6.27	Zr-96	Zr	30	4	0.25185148
97	42	6.19	Mo-97	Mo	30.98	3	0.18647855
137	55	6.16	Cs-137	Cs	6.16	1	0.06185826
99	42	6.14	Mo-99	Mo	30.98	3	0.18497226
141	58	6.08	Ce-141	Ce	18.28	3	0.18316471
143	60	5.89	Nd-143	Nd	22.567	3	0.17744082
91	40	5.88	Zr-91	Zr	30	4	0.23618608
142	58	5.88	Ce-142	Ce	18.28	3	0.17713956
98	42	5.84	Mo-98	Mo	30.98	3	0.17593453
90	38	5.81	Sr-90	Sr	14.12	2	0.11668717
144	60	5.38	Nd-144	Nd	22.567	3	0.16207667
92	40	5.06	Zr-92	Zr	30	4	0.20324856
101	44	5	Ru-101	Ru	15.245	3	0.15062888
89	38	4.74	Sr-89	Sr	14.12	2	0.09519745
132	54	4.31	Xe-132	Xe	31.72	0	0
102	44	4.16	Ru-102	Ru	15.245	3	0.12532322
145	60	3.87	Nd-145	Nd	22.567	3	0.11658675
88	38	3.57	Sr-88	Sr	14.12	2	0.07169934
103	44	2.99	Ru-103	Ru	15.245	3	0.09007607
146	60	2.94	Nd-146	Nd	22.567	3	0.08856978
131	53	2.92	I-131	I	2.92	0	0
87	37	2.52	Rb-87	Rb	3.84	2	0.0506113
147	60	2.18	Nd-147	Nd	22.567	3	0.06567419
130	51	1.99	Sb-130	Sb	3.216	0	0
86	36	1.88	Kr-86	Kr	3.389	0	0
104	44	1.8	Ru-104	Ru	15.245	3	0.0542264
148	60	1.66	Nd-148	Nd	22.567	3	0.05000879
85	37	1.32	Rb-85	Rb	3.84	2	0.02651068
149	61	1.04	Pm-149	Pm	1.04	3	0.03133081
129	51	0.996	Sb-129	Sb	3.216	0	0
84	36	0.967	Kr-84	Kr	3.389	0	0
105	44	0.897	Ru-105	Ru	15.245	3	0.02702282
150	60	0.647	Nd-150	Nd	22.567	3	0.01949138

[4] Information on UF_4 fission fragment fractional yields courtesy of Ron Lipinski of Sandia National Laboratories.
[5] Isotope mass (A), atomic number (Z), and Yield adapted from (Gorur, 1989; Vandenbosch, 1973).
[6] Isotope mass (A), atomic number (Z), and Yield adapted from (Gorur, 1989; Vandenbosch, 1973).
[7] Information on element yield, fluoride coordination number, and fluorine requirement courtesy of Dr. Lloyd Brown of General Atomics.

TABLE B–3 (Continued)[8]

A (amu)[9,10]	Z (e)	Yield (%/amu)	Isotope Symbol	Element Symbol	Element Yield[11]	Fluorine Coordination No.	Fluorine Requirement
83	36	0.542	Kr-83	Kr	3.389	0	0
128	50	0.458	Sn-128	Sn	0.517	0	0
151	62	0.418	Sm-151	Sm	0.878	3	0.01259257
106	44	0.398	Ru-106	Ru	15.245	3	0.01199006
82	34	0.319	Se-82	Se	0.569	0	0
152	62	0.239	Sm-152	Sm	0.878	3	0.00720006
107	45	0.189	Rh-107	Rh	0.189	3	0.00569377
153	62	0.157	Sm-153	Sm	0.878	3	0.00472975
81	34	0.147	Se-81	Se	0.569	0	0
127	51	0.137	Sb-127	Sb	3.216	0	0
80	34	0.103	Se-80	Se	0.569	0	0
108	46	0.075	Pd-108	Pd	0.115	0	0
154	62	0.064	Sm-154	Sm	0.878	3	0.00192805
126	51	0.064	Sb-126	Sb	3.216	0	0
79	33	0.056	As-79	As	0.084	0	0
155	63	0.031	Eu-155	Eu	0.055	3	0.0009339
109	46	0.03	Pd-109	Pd	0.115	0	0
125	51	0.029	Sb-125	Sb	3.216	0	0
78	33	0.02	As-78	As	0.084	0	0
110	47	0.02	Ag-110	Ag	0.051	0	0
111	47	0.019	Ag-111	Ag	0.051	0	0
124	50	0.017	Sn-124	Sn	0.517	0	0
123	50	0.015	Sn-123	Sn	0.517	0	0
121	50	0.014	Sn-121	Sn	0.517	0	0
122	50	0.013	Sn-122	Sn	0.517	0	0
156	63	0.013	Eu-156	Eu	0.055	3	0.00039164
113	47	0.012	Ag-113	Ag	0.051	0	0
120	49	0.011	In-120	In	0.033	0	0
119	49	0.011	In-119	In	0.033	0	0
118	49	0.011	In-118	In	0.033	0	0
117	48	0.011	Cd-117	Cd	0.042	0	0
114	48	0.011	Cd-114	Cd	0.042	0	0
112	46	0.01	Pd-112	Pd	0.115	0	0
116	48	0.01	Cd-116	Cd	0.042	0	0
115	48	0.01	Cd-115	Cd	0.042	0	0
77	33	0.008	As-77	As	0.084	0	0
157	63	0.007	Eu-157	Eu	0.055	3	0.00021088
158	63	0.004	Eu-158	Eu	0.055	3	0.0001205
76	32	0.002	Ge-76	Ge	0.003	0	0
160	65	0.001	Tb-160	Tb	0.001	3	3.0126E-05
75	32	0.001	Ge-75	Ge	0.003	0	0
159	64	0.001	Gd-159	Gd	0.001	3	3.0126E-05
72	30	0	Zn-72	Zn	0	0	0
161	65	0	Tb-161	Tb	0.001	3	0
74	31	0	Ga-74	Ga	0	0	0
73	31	0	Ga-73	Ga	0	0	0

[8] Information on UF_4 fission fragment fractional yields courtesy of Ron Lipinski of Sandia National Laboratories.
[9] Isotope mass (A), atomic number (Z), and Yield adapted from (Gorur, 1989; Vandenbosch, 1973).
[10] Isotope mass (A), atomic number (Z), and Yield adapted from (Gorur, 1989; Vandenbosch, 1973).
[11] Information on element yield, fluoride coordination number, and fluorine requirement courtesy of Dr. Lloyd Brown of General Atomics.

B.3. Fission Product Properties

B.3.1. Xenon[12]

MW = 131.29	P_{crit} = 57.63997 atm
T_{nbp} = 165.03 K	V_{crit} = 118 cc/mol
T_{mp} = 161.36 K	ω = 0
T_{crit} = 289.74 K	Z_{crit} = 0.286

Extended Antoine's Equation in Aspen Plus

$$\ln P(atm) = 29.4089115 - \frac{1865.9}{T} - 3.90\ln T + 0.011049\,T,\ (161 - 290\ K) \quad .$$

B.3.2. Molybdenum Hexafloride

MW = 209.93	ω = 0.649
T_{nbp} = 307.15 K[13]	V_{crit} = 237.9 cc/mol
T_{mp} = 290.55 K	V_b = 87.95 cc/mol
T_{crit} = 431 K	Z_{crit} = 0.286
P_{crit} = 35.5 atm	

Extended Antoine's Equation

$$\log P(\text{mmHg}) = -\frac{1499.9}{T} + 7.766,\ (17° - 34°\text{C}) \quad .$$

Extended Antoine's Equation in Aspen Plus

$$\log P(\text{mmHg}) = 46.49734 - \frac{4703.74}{T} - 4.28004\ln T,\ (290 - 400\,\text{K}) \quad .$$

[12] All properties from Aspen Plus inorganic databank for xenon.
[13] Scalar properties (excluding critical) and Antoine's equation adapted from (Canterford, 1968).

B.3.3. Zirconium Tetrafluoride

MW = 167.218	ω = 1.338
T_{nbp} = 1185.15 K[14]	V_{crit} = 156 cc/mol
T_{mp} = 1205.15 K	V_b = 40.17 cc/mol
T_{crit} = 1665 K	Z_{crit} = 0.1839
P_{crit} = 161.1 atm	

Extended Antoine's Equation

$$\log P(\text{mmHg}) = -\frac{12376.0}{T} + 13.3995,\ (617 - 881\text{K})^{15} \quad .$$

Extended Antoine's Equation in Aspen Plus

$$\log P(\text{mmHg}) = 30.859 - \frac{28501.9}{T},\ (889 - 1154\,\text{K}) \quad .$$

B.3.4. Neodymium Trifluoride

MW = 201.235	ω = 1.794
T_{nbp} = 2573 K[16]	V_{crit} = 114.6 cc/mol
T_{mp} = 1647 K	V_b = 87.95 cc/mol
T_{crit} = 3591 K	Z_{crit} = 0.1475
P_{crit} = 379.3 atm	

Extended Antoine's Equation

$$\log P(\text{atm}) = -\frac{18730}{T} + 8.03,\ (1383 - 1520\,\text{K})^{17} \quad .$$

Extended Antoine's Equation in Aspen Plus

$$\log P(\text{atm}) = 18.5 - \frac{43135}{T},\ (1383 - 1520\,\text{K}) \quad .$$

[14] T_{nbp} and T_{mp} adapted from (Winter, 2001).
[15] Extended Antoine's equation adapted from (Sense, 1963).
[16] T_{nbp} and T_{mp} adapted from (Winter, 2001).
[17] Extended Antoine's equation adapted from (Brown, 1968).

B.3.5. Cerium Trifluoride

MW = 197.11	ω = 1.735
T_{nbp} = 2600 K[18]	V_{crit} = 118.6 cc/mol
T_{mp} = 1703 K	V_b = 34.07 cc/mol
T_{crit} = 3251 K	Z_{crit} = 0.1522
P_{crit} = 342 atm	

Extended Antoine's Equation

$$\log P(\text{atm}) = -\frac{20460}{T} + 9.205,\ (1373 - 1634\,\text{K})^{19} \ .$$

Extended Antoine's Equation in Aspen Plus

$$\log P(\text{atm}) = 21.2 - \frac{47120}{T},\ (1373 - 1534\,\text{K}) \ .$$

B.3.6. Strontium Difluoride

MW = 125.617	ω = 1.772
T_{nbp} = 2733 K[20]	V_{crit} = 123.6 cc/mol
T_{mp} = 1746 K	V_b = 31.53 cc/mol
T_{crit} = 3823 K	Z_{crit} = 0.1493
P_{crit} = 379 atm	

Extended Antoine's Equation

$$\log P(\text{Pa}) = -\frac{47466}{T} + 30.40,\ (1381 - 1720\,\text{K})^{21} \ .$$

Extended Antoine's Equation in Aspen Plus

$$\log P(\text{atm}) = 23.49 - \frac{47466}{T},\ (1381 - 1720\,\text{K}) \ .$$

[18] T_{nbp} and T_{mp} adapted from (Winter, 2001).
[19] Extended Antoine's equation adapted from (Lim, 1966).
[20] T_{nbp} and T_{mp} adapted from (Winter, 2001).
[21] Extended Antoine's equation adapted from (Zaitsev, 1990).

B.4. Literature Cited

Anghaie, S., "Thermophysical Properties of UF_4 at High Temperatures ($1000 \leq T \leq 10{,}000$ K)," available online at: http://www.inspi.ufl.edu/data/uf4_properties.pdf, last accessed 28 September 2001.

Brown, D., J.H. Canterford, and R. Colton, *Halides of the Transition Elements, Halides of the Lanthanides and Actinides*, Wiley, London, (1968-69).

Canterford, J.H. and R. Colton, *Halides of the Transition Elements, Halides of the Second and Third Row Transition Metals*, Wiley, New York, (1968).

Gorur, R., "Stopping and Relaxation Spectrum of Uranium Fission Fragments with a Monte Carlo Analysis of Energy Deposition of the Containment Surface of a Gas Core Reactor," Thesis, U. of Florida, 1989.

Green, P., *Perry's Chemical Engineer's Handbook on CD-ROM*, McGraw Hill Companies Inc., New York, p.4-36 (1999).

Hakuta, T., and M. Hirata, "Estimation of Critical Constants," *Journal of Chemical Engineering of Japan* **3**(1), 5 (1970).

Lim, M. and A.W. Searcy, "Vapor Pressure and Heat of Sublimation of Cerium (III) Fluoride," *J. of Phys. Chem.* **70**, 1762-5 (1966).

Sense, K.A., M.J. Snyder, and R.B. Filbert Jr., "The Vapor Pressure of Zirconium Fluoride," *J. Inorg. Chem.* **8**(6), 789-90 (1963).

Smith, J.M., H.C. Van Ness, and M.M. Abbott, *Introduction to Chemical Engineering Thermodynamics, Fifth Edition*, McGraw-Hill Companies Inc., New York (1996).

Vandenbosch, R. and J.R. Huizenga, *Nuclear Fission*, Academic Press, New York (1973).

Winter, M., "WebElements™ Professional Edition," available on-line at: http://www.webelements.com/, last accessed 30 September 2001.

Zaitsev, A.I., N.V. Korolyov, B.M. Mogutnov, "Vapor Pressure and Heats of Sublimation of CaF_2 and SrF_2," *High Temperature Science* **28**, 341 (1990).